POLITECNICO DI TORINO

Department of Environment, Land and Infrastructure Engineering

Master of Science in Petroleum Engineering

Nacer Benlalam

Sensitivity of the Virtual Element Method to volume discretization when simulating the subsidence phenomena

Thesis submitted in compliance with the requirements for
the Master of Science degree

Supervisor:
Prof. Francesca VERGA
Co-Supervisor:
Dott. Cristina Serazio

March 2020

The page is left intentionally blank.

ACKNOWLEDGEMENT

I would like to express my deep and sincere gratitude to my supervisor Professor Francesca Verga for giving me the opportunity to do research on this invaluable project.

I would like to sincerely thank my co-supervisor Cristina Serazio for her time dedicated into helping me with my thesis work, and the massive efforts she generously given me during this process.

Special thanks to Professor Vera Rocca for her guidance and support.

I am extending my thanks to the Petroleum Engineering group staff in the Department of Environment, Land and Infrastructure Engineering, for their kindness.

I am extremely grateful to my parents and siblings for their encouragement and unconditional support.

DÉDICACES

Mon but dans la vie avant toute chose a toujours été d'emplir mes parents de fierté et de satisfaction, en signe de reconnaissance pour tout ce qu'ils ont consenti comme efforts et sacrifices afin de me voir réussir. Je dédie donc ce modeste travail.

Aucune dédicace ne pourrait exprimer mon respect, ma considération et mes profonds sentiments envers eux.

A mon cher frère « AMINE » à qui je souhaite beaucoup de réussite et ma petite sœur « KAHINA » qui m'encourage régulièrement et à qui je souhaite plein de bonheur.

NACER

SUMMARY

INDEX OF FIGURES:

INDEX OF TABLES:

LIST OF SYMBOLS:

σ_{ij}	Stress tensor
C_{ijkh}	Stiffness tensor
ε_{kh}	Strain tensor
σ	Normal Stress
τ	Shear Stress
ε	Normal Strain
Γ	Shear strain
E	Young modulus
ν	Poisson ratio
G	Shear modulus
λ	Lamé’s coefficient
K	Bulk modulus
σ’	Effective stress
P	Pressure
α	Biot coefficient
K_{fr}	Bulk modulus of material’s framework
K_s	Bulk modulus of the solid grains
ε^e	Elastic strains
ε^p	Plastic strains
e	Void ratio
υ	Specific volume
V_v	Volume of pores
V_s	Volume of solid
p'_c	Preconsolidation Stress
OCR	Overconsolidation ratio
E_{fr}	Young modulus of material’s framework
σ'_h	Minimum horizontal effective stress
σ'_H	Maximum horizontal effective stress
σ'_v	Vertical effective stress
ν_{fr}	Poisson ratio of the framework
ε_h	Horizontal strain
ε_v	Vertical strain
P_f	Fluid pressure
C_m	Uniaxial compaction
γ	Stress path coefficient.
γ_v	Vertical stress path coefficient
γ_h	Horizontal stress path coefficient
u_0	Radial displacement at the surface of a unit sphere
R_0	Radius of the sphere
r	Distance from the center of the sphere
$[K]$	Stiffness matrix
$[E]$	Flow matrix
$[L]$	Coupling matrix between the mechanical and flow unknowns

$\vec{F}$	Vector of Force of boundary conditions
$\vec{R}$	Residual of the flow equations
$\vec{\delta}$	Vector of displacements
$\vec{P}$	Vector of the reservoir unknowns
$\Delta_{\boldsymbol{t}}$	Variation per time step
ρ	Density
e_{rel}	Absolute norm relative error
dz	Vertical displacement
NTG	Net gross

ABSTRACT

In primary production/UGS context, geomechanical modeling is aimed at evaluating the system safety in terms of reservoir and cap rock integrity, induced subsidence/rebound and existing faults (re)activation. To this end a discretized model able to describe the volume of interest is usually constructed and numerical simulations are performed to assess the displacement of the mesh nodes and the stress variation. Traditionally such calculations are performed through the well-established Finite Element Methods (FEM). In the present work, the Virtual Element Method (VEM) a generalization of FEM to polyhedral meshes was tested on *ad hoc* constructed 3D models and results were compared against solution obtained from FEM simulation. Sensitivity and limitations of the implemented VEM with respect to the selected grid were analyzed.

Keywords: Virtual element method, Subsidence, Reservoir simulation, Corner point grids, Unstructured grids, Linear elasticity.

1. INTRODUCTION

Most of Geomechanical applications fall under the umbrella of safety analysis and prevention. More specifically exploration and exploitation of deepwater fields need a careful planning considering the corresponding expensive high rate wells and platforms. In primary production context, most reservoirs are multi-layered, over pressurized and have weakly cemented sands and silt sequences. Thus, a large pressure depletion can lead to large rock deformations and primarily compaction at the reservoir level, and associated surface subsidence that is responsible for a number of field operating problems. Hence, it’s imperative to carry out Geomechanical studies on the impact of reservoir operations to evaluate the system safety in terms of the reservoir and cap rock integrity, the induced subsidence/rebound and existing faults (re)activation. The results of these studies assist decision makers (engineers, operators, economists…etc) in crafting a fitting strategy for an optimal field development and management.

The integration of a geomechanical study in a typical petroleum engineering workflow requests the construction of a 3D full-field model and the simulation of the response of the system to the production activities with the intrinsic challenge in balancing between accuracy and computation effort to calculate the solution considering that typically a geomechanical model can be significantly larger than a reservoir model. This is the reason why computation efficiency is critical in this case. Several numerical solutions can be found in technical literature which provide a compromise between economical requirements and numerical feasibility

Traditionally, commercial softwares dedicated to geomechanical applications implement Finite Element approaches (FEM). Therefore, the model construction process is coherent with its theoretical framework. As an example, volume discretization strategies, data extrapolation schemes, and the set-up of boundary conditions are mainly adapted for the Finite Element Method.

In the present work, the Virtual Element Method (VEM) a newly presented numerical method defined as a generalization of FEM to polyhedral meshes is applied to a realistic geomechanical test case. In particular the VEM solution is compared against the FEM commercial software solution provided by Schlumebrger Geomechanics®. At this stage of the project, a prototype code is available for the computation of field displacements

induced by pressure depletion within the elastic domain from an independent source input.
At first, we devised a strategy to properly construct models for the VEM simulation which are equivalent of the FEM oriented models (by taking advantage of the options offered by FEM commercial software).
Secondly we observed that certain details relating to data pre-processing and solver implementation of the FEM commercial software are inaccessible to the user due to software licensing and confidentiality, thus we defined a simplified synthetic model in order to confine the solution discrepancies between the two methods to different implementation strategies that cannot be reproduced using the VEM prototype. As an initial goal, we expected to quantify a minimum solution discrepancy for future references, when simulating realistic models.
Finally, we tested the VEM over different discretizations of the same volume under the same set of inputs. Initially, in compliance with the VEM theoretical framework, the simulation was performed on a tetrahedral grid, where we expected the output to be reliable and representative of the subsidence phenomena. Next, we computed the VEM over the same “corner point grid” adopted by the commercial software. From the results analysis we probed the areas where the discrepancies were prominent and tried to single out the possible sources. Based on our assessment we modified the grid and prepared a new discretization scheme ready for the next simulation. We re-iterated these steps until an acceptable prediction of subsidence phenomena is approximated. Our main results concerned the assessment of the VEM dependency on volume discretizations, we tested its sensitivities within the frame of our model while conjointly provided a strategy to treat the confronted limitations.

2. LITERATURE REVIEW

Within the framework of Geomechanics, the establishment of the mechanics of deformable solids and porous sedimentary environments is of main interest. The subject englobes a variety of disciplines aiming for building the constitutive behavior of materials when exposed to ever changing loading conditions: stresses, pressures, temperatures and chemistry.

The scope of our work is the comparison of two numerical methods in approximating the solution of the geomechanical application: depletion-induced subsidence within the elastic frame. The latter is delimited by a threshold under which any mechanical deformation the material underwent can be recovered if the initial conditions were satisfied again. Any strain occurring outside of the elasticity limit is considered plastic and can’t be retrieved. The concept of elastic behavior is rather complex taking into account its dependence on material mechanical (elastic) properties, testing conditions and state of stress.

We would consider the discrete nature of materials and develop certain concepts of elasticity and define particular properties used in the characterization of constitutive performance of porous material (Poro-elasticity).

Subsequently, we examine the reservoir’s response to hydrocarbon production and how the mechanical disturbance travels to its surroundings. In addition, we explore an analytical evaluation of the compaction and subsequent subsidence problem based on Geertsma’s nucleus of strain model.

Next, we approach the geomechanical modelling main considerations: Reservoir dynamic simulation and its modelling components are briefly examined, the extension of the solution domain and the definition of the different theoretical approaches used in coupling fluid-flow and rock mechanics to reproduce the stress-strain deformation.

We explore briefly Finite element and Virtual element methods, with a mention on how they solve elasticity problems.

2.1. Constitutive laws:

A constitutive law is an ensemble of equations describing the relationship between applied stresses on a rock medium and its consequent deformation. Evidently, this conceptualization is the umbrella for a wide variety of physical behaviors, therefore, we will be addressing certain key principles, parameters and examples relating to the theory of elasticity and poroelasticity.

2.1.1. The Theory of Elasticity [1][2]:

The term «elastic» is used to underline the notion that a loaded Fig. 2.1 or a strained body possess a potential energy [2] that may be released during unloading causing it to rebound to its original shape. To describe this behavior, Constitutive laws take into account the mechanical properties of the materials.

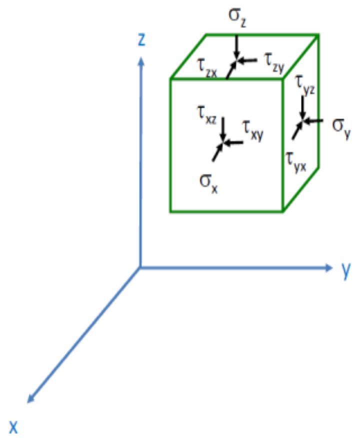

Fig. 2.1: Stresses acting on a finite parallelepipedal volume.

The relationship that describes this behavior relating directly the infinitesimal stresses to the infinitesimal strains can be written as such Eq. (2.1):

$$d\sigma_{ij} = C_{ijkh} d\varepsilon_{kh} \tag{2.1}$$

C is designated as the stiffness tensor, which is the ensemble of independent scalars relating the stresses to the consequent strains referred to as elastic constants.

The response of a material when loaded Fig. 2.1 within its elastic limit manifests under several scenarios Fig. 2.2 depending on the magnitude of stress applied, the elastic properties and the stress history of the material. Even though, bearing formations are subjected to large stresses that may induce non-linear responses, it's still possible to analytically describe their behavior through linear relations if the applied stresses changes in an infinitesimal manner.

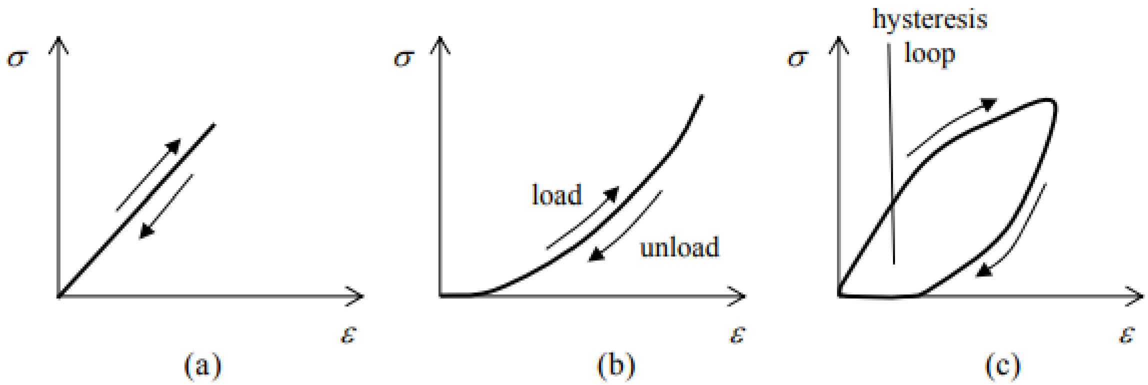

Fig. 2.2: Different stress-strain relationships: (a) Linear elastic (b) Non-linear elastic (c) Hysteresis.

The most well-known constitutive law is the Generalized Hooke's law Eq. (2.2). for the behavior of an isotropic[1] linear elastic material, characterized by the use of only two elastic parameters E young Modulus and υ Poisson's ratio.

$$\begin{bmatrix} \sigma_x \\ \sigma_y \\ \sigma_z \\ \tau_{xy} \\ \tau_{yz} \\ \tau_{zx} \end{bmatrix} = \frac{E(1-\upsilon)}{(1+\upsilon)(1-2\upsilon)} \begin{bmatrix} 1 & \frac{\upsilon}{1-\upsilon} & \frac{\upsilon}{1-\upsilon} & 0 & 0 & 0 \\ \frac{\upsilon}{1-\upsilon} & 1 & \frac{\upsilon}{1-\upsilon} & 0 & 0 & 0 \\ \frac{\upsilon}{1-\upsilon} & \frac{\upsilon}{1-\upsilon} & 1 & 0 & 0 & 0 \\ 0 & 0 & 0 & \frac{1-2\upsilon}{2(1-\upsilon)} & 0 & 0 \\ 0 & 0 & 0 & 0 & \frac{1-2\upsilon}{2(1-\upsilon)} & 0 \\ 0 & 0 & 0 & 0 & 0 & \frac{1-2\upsilon}{2(1-\upsilon)} \end{bmatrix} \begin{bmatrix} \varepsilon_x \\ \varepsilon_y \\ \varepsilon_z \\ \Gamma_{xy} \\ \Gamma_{yz} \\ \Gamma_{zx} \end{bmatrix} \tag{2.2}$$

[1] Isotropic material: When subjected to a state of stress, the material's response is independent of the orientation of the applied stress.

2.1.1.1.Elastic Parameters [1]:

The coefficients correlating the stress and the elastic responses of the material are grouped as ***"elastic moduli"***:

- ***Young Modulus E**:* is a measure of the stiffness of the material Eq. (2.3), it's estimated through uniaxial stress tests, where the product of the modulus to the lateral strain is equal to the perpendicular applied stress.

$$\sigma = E\varepsilon \tag{2.3}$$

- ***Poisson's ratio ν*** : Eq. (2.4), the lateral expansion to the longitudinal shortening.

$$\nu = -\frac{\varepsilon_y}{\varepsilon_x} \tag{2.4}$$

- ***Lame's Parameters:***

  ***Shear modulus G**:* it quantifies the material's resistance against shear deformations Eq. (2.4). It is physically estimated as the ratio of the applied shear stress to its shear strain.

$$G = \frac{E}{2(1+\nu)} \tag{2.4}$$

  Lame's Constant : Eq. (2.5)

$$\lambda = \frac{\nu E}{(1+\nu)(1-2\nu)} \tag{2.5}$$

- ***Bulk Modulus K*:** it quantifies the material's resistance against hydrostatic loading Eq. (2.6), consequently the inverse 1/K is representative of the compressibility.

$$\mathrm{K} = \lambda + \frac{2}{3}\mathrm{G} \tag{2.6}$$

The determination of elastic moduli can be a challenging process, as it can present a significant discrepancy depending on the methodology used to estimate them. We can group them as *Dynamic moduli* measured through acoustic velocities or *Static moduli* obtained from stress/strain measurements. Evidence have shown that the heterogeneous discrete nature of rocks is one of the main sources for such differences. This underlines that the depositional history, stress-strain history and rock types are defining factors for the value of elastic parameters.

Tab. 2.1: Static mechanical properties for some common rock types.

Material	Density ρ 10^3 (kg/m^3)	Young's modulus E (GPa)	Poisson's ratio ν
Unconsolidated sands	1.5–1.7	0.01–0.1	~0.45
Sandstone	2.0–2.65	0.1–30	0–0.45
Clay	1.9–2.1	0.06–0.15	~0.40
Shale	2.3–2.8	0.4–70	0–0.30
High porosity chalk	1.4–1.7	0.5–5	0.05–0.35
Low porosity chalk	1.7–2.0	5–30	0.05–0.30
Basalt	2.7–2.9	50–100	0.2–0.3
Granite	2.6–2.8	5–85	0.1–0.34
Dolomite	2.4–3.2	10–100	0–0.5
Limestone	1.4–2.9	2–100	0–0.3
Gneiss	2.7–3.1	40–100	0.1–0.3
Marble	2.7–3.2	5–90	0–0.3
Ice	0.9	8	0.35
Steel	7.9	200	0.28

2.1.2. Poro-Elasticity [1] [2] [3] [4] [5]:

The theory of Poro-elasticty lays the grounds for constitutive models which describe the mechanical behavior of saturated rocks/soils when subjected to external load. Highlighting the role of void space in both fluid flow and the deformation of the containing material. The work, on which the theory was based on, was first initiated by K. Terzaghi 1925, aiming to study the process of soil consolidation under the assumption that the grains forming the soil are bounded by certain molecular forces constituting an elastic porous material. Terzaghi performed this work on a fully saturated soil under oedometric conditions (one-dimensional deformations). In 1941, M Biot extended this approach to a three-dimensional problem where the porous material is subjected to arbitrary loads.

To account for poroelastic effects of material loading, certain assumptions have to be made first:

- Interconnected pore system fully saturated.
- Total Pore volume of the system is relatively smaller than the bulk volume.
- External and internal loads (total stress, pore pressure) uniformly act on the system as well as its internal grain structure.

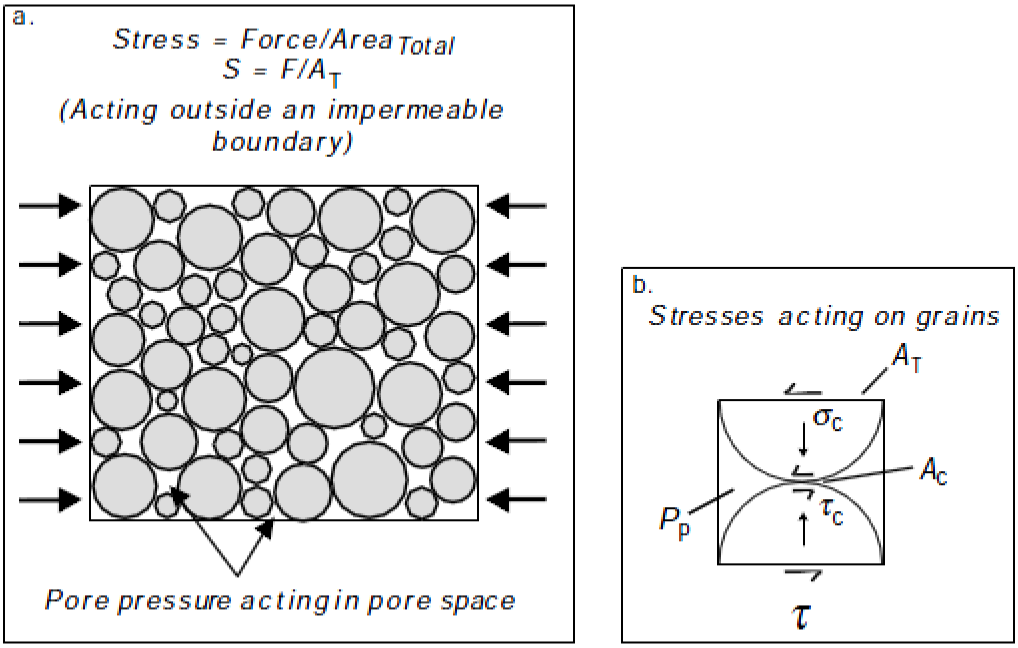

Fig. 2.3: a) Schematic illustration of a porous material on which an external load is applied outside an impermeable boundary, and pore pressure acting within the pore. b) Grain scale: Schematization of the force acting on the grains as the difference between the applied force and pore pressure (Terzaghi principle). [3]

Terzaghi states: when a saturated porous material is under a state of stress, the distributed loads are partly supported by the solid framework of the volume, and partly by the fluid within the pores. Notably, the total external stress applied is evened out partially by stresses on the skeleton and partially by a hydrostatic pressure. The potential energy of the strained poroelastic material is therefore influenced by the interstitial fluid within its pores. This is translated as "***the effective stress principle"*** Eq. (2.7)**.**

$$\sigma'_{ij} = \sigma_{ij} - \delta_{ij} P \tag{2.7}$$

Where σ_{ij} and σ'_{ij} are the total and effective stresses respectively while P is the pore pressure. The formulation Eq. (2.7) describes the coupled behavior of applied stresses and pressure variations, stating that any mechanical alterations occurring to the medium are solely due to effective stress changes.

By considering the physical aspect of the pore pressure level of effects on stresses acting on the solid framework, Biot has reformulated Terzaghi's principle by introducing the coefficient "α" Eqs. (2.8) and (2.9):

$$\sigma'_{ij} = \sigma_{ij} - \alpha\delta_{ij}P \tag{2.8}$$

Where:

$$\alpha = 1 - \frac{K_{fr}}{K_s} \tag{2.9}$$

$\boldsymbol{K_{fr}}$**:** is the bulk modulus of the framework of the material (skeleton), it's estimated through a hydrostatic drained (jacketed) test Fig. 2.4 done on a saturated material, where the pore pressure is kept constant. This is translated as any stress variation applied on the material is entirely carried by the framework allowing us to characterize the material's stiffness. In literature, "drained conditions" refer to permeable mediums where fluids are able to dissipate through when load is applied.

$\boldsymbol{K_s}$**:** is the bulk modulus of the solid grains. It's estimated through a hydrostatic undrained test (unjacketed) test Fig. 2.4 done on a saturated material. The test is conducted by applying confining loads on a porous material immersed fluid under pressure while holding the experiment under the condition$\Delta\sigma = \Delta P_f$. This means that resulting the stiffness measured is one of the solid grains. "Undrained conditions" refer to mediums where fluids are not able to escape, or when they need considerable amount of time to reach equilibrium again when loaded, 'impermeable media.

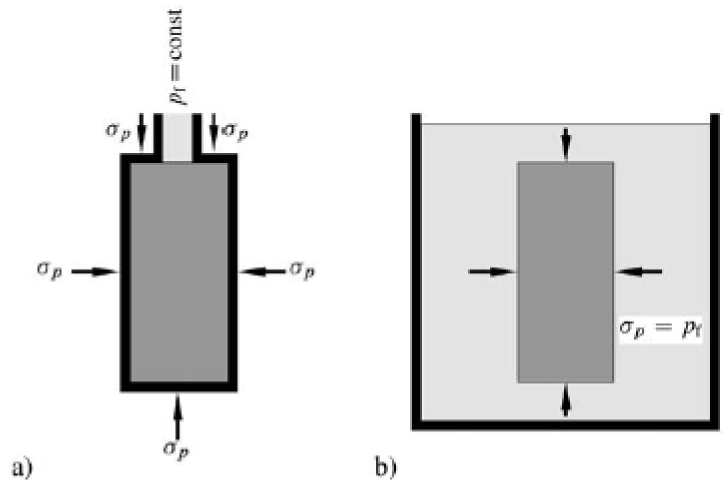

Fig. 2.4: Schematics of a) Drained test b) Undrained test [2].

With respect to Eq. (2.7) and Eq. (2.9), we have the possibility to describe in short the stress distribution and the effects of pore pressure with respect to stiff/weak framed rocks.

For weakly framed rocks "soils": the frame is highly compressible: $K_{fr} \ll K_s$ ➔ $\alpha \approx 1$ This validates Terzaghi's orginal work about soil consolidation, confirming that the soil's bulk modulus is also affected by the fluids' bulk modulus K_f .

***For stiff framed rocks*:** the frame has a low compressibility relative to that of the fluid$K_{fr} \gg K_f$. Where, the bulk modulus of the frame becomes comparable to that of its solid grains$K_{fr} \sim K_s$, reducing the value of the Biot coefficient α. Consequential reduction of pore pressure effects in supporting the applied stresses. For hard rocks, most of the loads are carried by their skeleton. From a geotechnical point of view, the bulk moduli of the frame and of the solid grains of hard rocks differ due to the heterogeneous nature of the minerals constituting the rock, it's possible to have the same value if it's formed of one type of minerals.

Now that we have established through the poroelasticity concept and Terzaghi principle: that the effective stress component is the one causing solid deformations, it's possible to rewrite the defined equations defined through the theory of elasticity by using the effective terms instead of total stresses while taking into account the dynamic/mechanical effects of fluid flow. This opens up a wide variety of scenarios: drained conditions, undrained conditions as well as the level of consolidation of material studied. Therefore, the elastic moduli that can be determined through these workflows are specific to the conditions under which the experiments were conducted.

2.1.3. Beyond the elasticity limit [2]:

The theory of placticity is the constitutive model used to describe the ductile[2] behavior of materials.When materials are stressed beyond their elastic limit ***"yield point"***, they undergo non recoverable deformations, where only a portion of the strains rebound back during unloading. Therefore the total strain asssociated to an applied stress can be described as the sum of elastic and plastic deformations Eq. (2.10):

$$\varepsilon = \varepsilon^e + \varepsilon^p \tag{2.10}$$

[2] Ductile behavior : it describes the space where the material undergoes permanent deformations without losing its ability to support the load.

As a result of continuous complex geological, mechanical and biological processes, in-situ rocks and soils vary greatly in terms of structures. Undisturbed samples when subjected to loading, their response seems to be greatly affected by such history. Modeling this analogous behavior of geomaterials requires the consideration of their dependencies to accurately predict their response. Weak sedimentary rocks display unique behavior when loaded, as they depend greatly on their structure. They are intermediate between hard rocks and soils, characterized by little to no cementation between individual grains. It has been established that Cam clay (soil mechanics) can be modified to be able to properly describe their mechanical behavior with respect to the administered loading conditions [2].

2.1.3.1.The CAM-Clay Model [2] [4] [5]:

Originally, during sedimentary and weathering processes, soil deposits undergo a series of loading and unloading sequences Fig. 2.5. During the deposition process A-B-C, the additional weight of overburden causes an increase of effective vertical stress, loose sediments will consolidate inducing a reduction of the void element (reduction of void ratio). The segment D-C representing the erosion process is translated as a reduction of the applied effective vertical load followed by a consequential decrease of void ratio. The graph shows evidence of residual strain after unloading, for the same effective overburden the points B and D exhibit different void ratios. This behavior sets certain singularities of the soils' mechanical responses***: its non-linear stress-strain response, its stress dependent stiffness and the exhibition of irreversible deformations without necessarily fulfilling failure conditions.***

Void ratio e*:* it is the relative void volume related to that of solid volume Eq. (2.11):

$$e = \frac{V_v}{V_s} \tag{2.11}$$

Specific Volume υ: total value divided by solid volume Eq. (2.12):

$$\upsilon = \frac{V_s + V_v}{V_s} = 1 + e \tag{2.12}$$

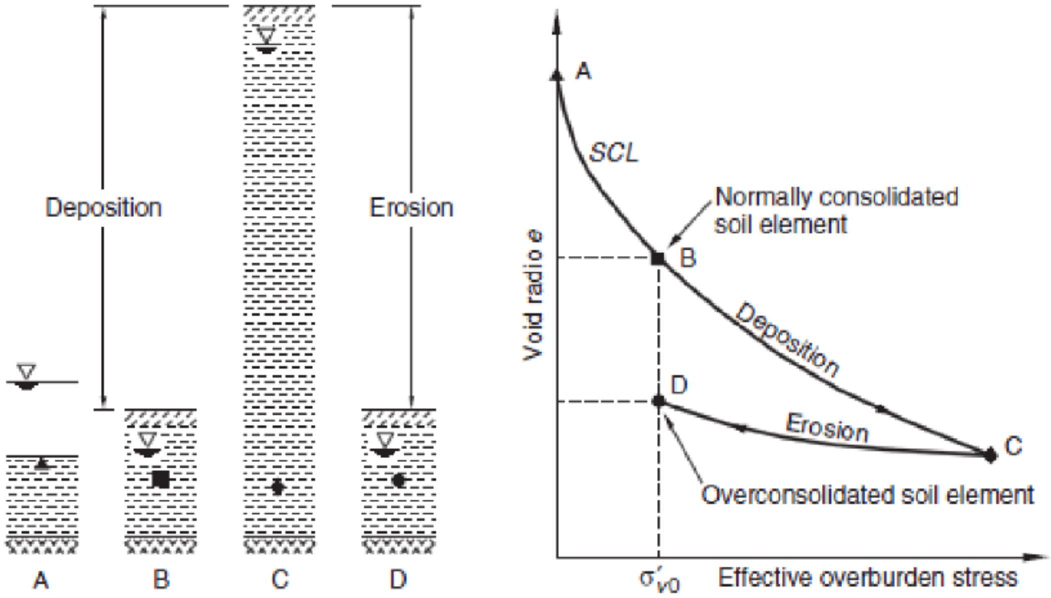

Fig. 2.5: Observed void ratio evolution under the effect of loading and unloading sequences of a soil deposit sample [5].

When a soil is exclusively consolidated by a gradual increase of effective overburden stress, it is said to be *"**Normally Consolidated**"*, its stress-strain behavior is primarily *elasto-plastic*. The highest stress at which the soil was geologically subjected to is described as *"**Preconsolidation Stress p'_c**"*. When the same soil goes through a phase of unloading it's now called **"*Overly Consolidated*"** as it exhibits a degree of swelling but it reaches a lower void ratio than an NC soil for the same level of applied effective stress.

The model is based under the conduction of laboratory triaxial tests "isotropic loading" on unconsolidated soils (ex: soft clays). The diagram Fig. 2.6 below shows the response of a series of isotropic loading/unloading of clay under drained conditions.

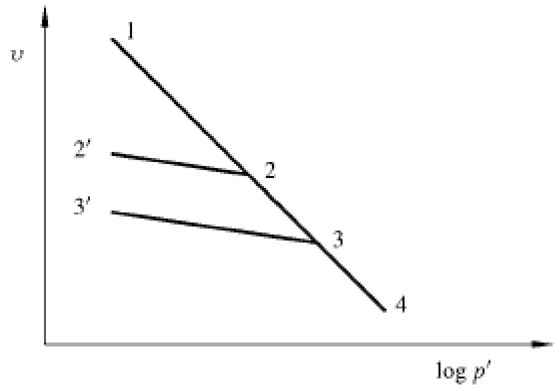

Fig. 2.6: Schematic isotropic compression of clay [5].

From the diagrams, it's possible to infer that the slope of NC soil is relatively more important that the OCs : this is reflected by a higher reduction of specific volume when exposed to the same load increment, which allows us to conclude that the stiffness of OCs is relatively greater than NCs.

In order, to determine the level of consolidation of the soils we are handling, we refer to the quantity ***"Overconsolidation Ratio" OCR*** *Eq. (2.13):* ratio between Preconsolidation stress and the current stress at which the soil is subjected to. When OCR=1 the soils are NC, when OCR>1 we have OC soils.

$$OCR = \frac{p'}{p'_c} \tag{2.13}$$

Moreover, normally consolidated soils have a unique relationship between specific volume and the exerted effective stress. As opposed to overly consolidated soils who follow different paths depending on the void ratio and the Preconsolidation stress from which the material was unloaded.

2.2.Reservoir Geomechanics:

Most of geomechanics applications fall under the umbrella of safety analysis and prevention. The most well-known example for mechanical effects caused by reservoir production is reservoir compaction as well as the associated surface subsidence. It can generate operational challenges endangering the well-being of field operations on a small scale or even bring forth environmental concerns on a larger scale.

A proper understanding of the physics behind such phenomena goes conjointly with the continuous development quest for better and more reliable engineering and computational tools to simulate and predict the geomechanical behavior during the exploitation phase to further optimize the reservoir management workflow. [2]

2.2.1. Compaction physics and the associated subsidence:

Rocks are generally described as "composite materials", referring to their heterogeneity on a length scale that is comparable to the particle size. Meaning that the rock's behavior and its over-all response depend not only on the matrix response but also on the non-solid part of the material. This concept is covered under the umbrella of *"**the poroelastic theory**"* providing us the necessary platform on which we can study compaction and its associated phenomena. [2] (Chapter 1, 6, 12).

In simple terms, a reservoir is a porous medium that contains fluids (hydrocarbons and water) within its solid structure. When considering the geological criteria for fluid entrapment coupled with increasing depth of burial due to sedimentation, there is a possibility where fluid expulsion rate may be lower than the sedimentation rate causing an over-pressurization of fluids within the bearing formation. Such phenomenon Fig.2.7 is generally characterized by a contrasting high level of pressure compared to that of a normal hydrostatic condition for the same depth and weight of the overlaying strata stressing upon the porous media, as well as having different intrinsic properties (such as porosity and permeability). The reason behind such distinctive behavior is due to having both the fluid and the solid framework supporting the stresses acting on the rock, and the degree of support provided by each one. This concept was previously described as the effective stress principle Eq. (2.8).

During production, the fluid pressure will generally drop, leading to an increase of the effective stress according to the Eq. (2.8), this is translated as more load is now being carried by the reservoir rock, causing the rock itself to shrink, in other words the reservoir will compact. [2]

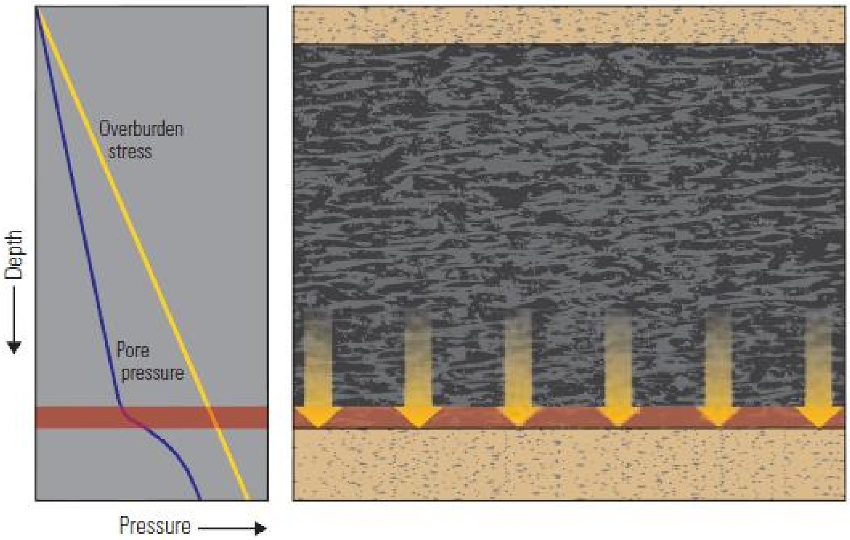

Fig. 2.7: The overburden stress (yellow arrows on the right) acting on the formation increases with depth due the added weight and is determined by density integration of the overburden (yellow line on the left). Similarly, the pore pressure (blue line on left) increases with a gradient determined by brine density. Beneath an impermeable layer (brown stripe), the pore fluid becomes overpressured as the formation compacts under additional overburden weight without being able to dissipate the pore fluid [6].

The resulting volume deformation of buried formation due to compaction is usually transmitted through the overburden Fig. 2.8 forming what is called a ***"subsidence bowl".*** The latter is wider than the compacted area [6][7].

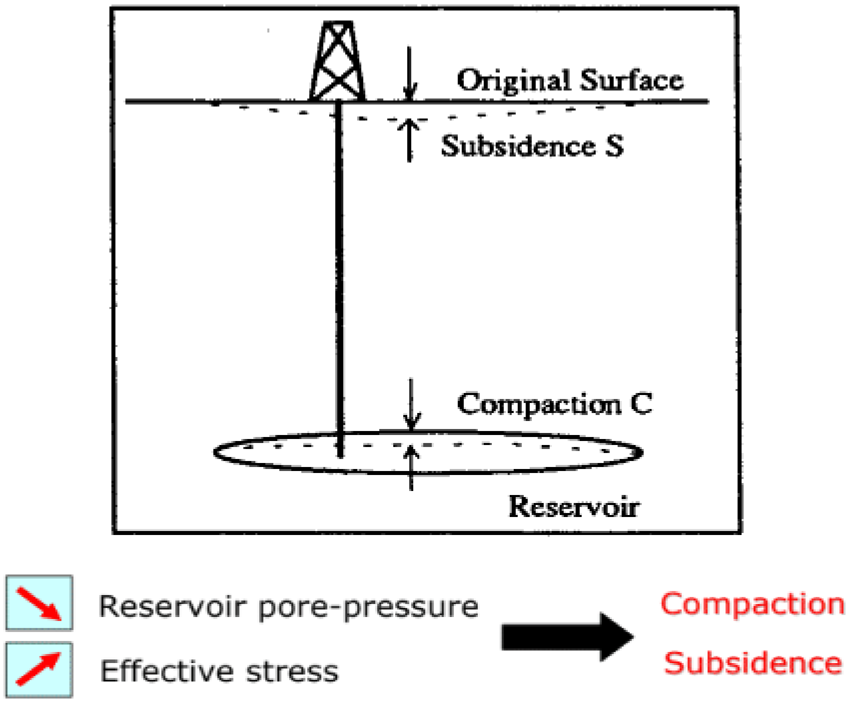

Fig. 2.8: Potential subsidence due to oil or gas withdrawal [2].

Evidently, all depleted oil/gas bearing formations will experience compaction, yet most will only witness small changes in volume and consequently a negligible surface subsidence. Following observations and evidence collected through the years, to have considerable amount of subsidence these following conditions must be fulfilled first [2] [8]:

- A significant reduction in reservoir pressure. (Any pressure maintenance mechanism will possibly counteract compaction).
- The bearing formation must be highly compressible, such as soft, loose or weakly cemented rocks.
- The reservoir must have a large vertical interval from which the production is effected (large thickness).
- The reservoir compaction must be significant, and not shielded by the overburden rock, which is why the depth and geometry of the reservoir

and the mechanical properties contrast between the reservoir and its surrounding plays a big part in the spread of subsidence bowl.

The compacting volume can be significantly larger if the aquifers beside or below the hydrocarbon bearing formation were affected, they may compact when their pressure is reduced.

When a formation undergoes compaction, the sideburden usually does not for two possible reasons: because it's impermeable and separated from the compacting region by non-communicating faults, or because it is a stronger more stiff material [7].

Another important point to consider is the motion with respect the subsidence bowl. Predominantly, the movement is vertical however horizontal movements also occur. The Land moves vertically down and horizontally toward the maximum pressure drop to what's called a *"reservoir gravity center*" which is where production wells are drilled. [7][33].

2.3.Practical Analytical solution for compaction and subsidence [2] [8] [9]:

Despite the general consensus in the engineering community, that numerical methods provide reliable and more accurate solutions, the analytical solutions are still of main interest because of their simple requirements and easy implementations to provide a general idea over the scale of compaction and the associated subsidence.

2.3.1. Reservoir compaction:

For the purpose of simplifying the solution for reservoir compaction, the reservoir volume reduction is assumed to be predominantly a result of height contraction. In technical terms, we can refer to it as a ***uniaxial reservoir compaction***. Furthermore, we under the hypotheses of: homogeneous isotropic reservoir, acting as linear elastic/poroelastic volume, and the absence of contrast between the reservoir and its surroundings. Evidently, the subsequent deformation of the rock can be expressed through the appropriate constitutive law: ***"Hooke's law"*** Eqs. (2.14) to (2.16) expressed in terms of stress variations with respect to the initial stress state (before depletion initiation):

$$E_{fr}\varepsilon_h = \Delta\sigma'_h - \nu_{fr}(\Delta\sigma'_H + \Delta\sigma'_V) \quad (2.14)$$

$$E_{fr}\varepsilon_H = \Delta\sigma'_H - \nu_{fr}(\Delta\sigma'_h + \Delta\sigma'_V) \quad (2.15)$$

$$E_{fr}\varepsilon_V = \Delta\sigma'_V - \nu_{fr}(\Delta\sigma'_H + \Delta\sigma'_h) \quad (2.16)$$

Provided that the lateral dimensions of the reservoir are large compared to its height. The variation of reservoir thickness Δh is given by the following relationship Eq. (2.17) between the vertical strain and the original thickness of the reservoir:

$$\Delta h = -\varepsilon_v h \quad (2.17)$$

Additionally. The stress evolution should be known to compute compaction, to do so certain assumptions must be imposed:

- For a lateral expansion larger than its vertical counterpart, we can consider the reservoir to only compact vertically, so it's possible to neglect horizontal strains Eq. (2.18):

$$\varepsilon_H = \varepsilon_h = 0 \quad (2.18)$$

- Second assumption is considering a constant total vertical load during production. This will result in the following equation Eq. (2.19) :

$$\Delta\sigma'_V = \Delta\sigma_V - \alpha\Delta\, P_f = -\alpha\Delta P_f \quad (2.19)$$

By introducing Eq. (2.18) into the Hook's law model, we can infer the necessity for vertical compaction to be maintained, the effective horizontal stresses must increase accordingly Eq. (2.20):

$$\Delta\sigma'_H = \Delta\sigma'_h = \frac{\nu_{fr}}{1-\nu_{fr}}\Delta\sigma'_v \quad (2.20)$$

Once we consider the previous assumptions within the generalized Hooke's law, the uniaxial compaction cab be expressed as such Eq. (2.21):

$$\frac{\Delta h}{h} = \frac{1}{E_{fr}} \frac{(1+\nu_{fr})(1-2\nu_{fr})}{1-\nu_{fr}} \alpha \Delta P_f \tag{2.21}$$

Or

$$\frac{\Delta h}{h} = C_m \alpha \Delta P_f \tag{2.22}$$

$\boldsymbol{C_m}$**:** Compaction coefficient/uniaxial compressibility.

From the resulting equations Eqs. (2.21) and (2.22) we can possibly quantify the reservoir's uniaxial compaction through three different individual influences:

- The reduction in reservoir pressure $\Delta P_f = P_{initial} - P_{final}$. (2.23)
- Vertical extent of the produced zone.
- The order of magnitude of the relevant mechanical properties of the reservoir formation.

Coherently, compaction defined as volumetric variation resulting from pore pressure depletion, it causes the reservoir to pull away relatively from the surface. Such behavior leads to a redistribution of vertical stresses Fig. (2.9) along the top reservoir as they decrease at the top of the reservoir and increase at its boundaries, in other terms they "***arch***". Accompanied with the lateral stress consideration previously mentioned, such phenomenon will affect displacement behavior with respect to pressure changes. It has become important to evaluate the stress evolution of the reservoir during production, in other words computing the reservoir's stress path.

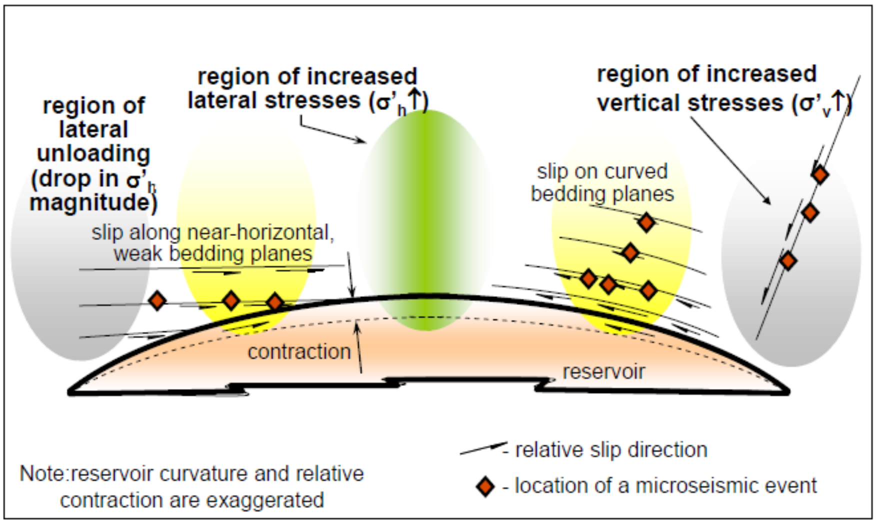

Fig. 2.9: Arching effect.

Within the frame of linear poro-elastic constitutive model previously presented, it's possible to introduce Stress Path Coefficients defined as follows Eqs. (2.23) to (2.25):

$$\gamma_v = \frac{\Delta\sigma_v}{\Delta P_f} \tag{2.23}$$

$$\gamma_h = \frac{\Delta\sigma_h}{\Delta P_f} \tag{2.26}$$

$$\gamma_H = \frac{\Delta\sigma_H}{\Delta P_f} \tag{2.25}$$

$\boldsymbol{\gamma_v}$**:** is also called the arching coefficient. Is equal to zero for uniaxial compaction.

It's possible to estimate the reservoir compaction for a general stress path Eqs (2.26):

$$\frac{\Delta h}{h} = \frac{\alpha}{E_{fr}}\left[\left(1-\frac{\gamma_v}{\alpha}\right) - 2\nu_{fr}\left(1-\frac{\gamma_h}{\alpha}\right)\right]\Delta P_f \tag{2.26}$$

It's necessary to highlight the fact that stress path coefficients are geometry dependent, in addition to the elastic contrast between the reservoir and its surroundings, emphasizing the dependency of the solution on the boundary conditions at the reservoir sides.

2.3.1.1.Compaction of a layered reservoir [2]:

For a layered material of isotropic layers of thickness h_i and total thickness h subjected to a normal load, under the assumption that all the layers must carry the same load. This type of media is modeled through the summation of the individual compaction of each layer i:

- The individual vertical strain per layer Eq. (2.27):

$$\varepsilon_{V,i} = \frac{\sigma_V}{E_i} = \frac{\Delta h_i}{h_i} \tag{2.27}$$

- The overall compaction of the material will then be as such Eq. (2.28):

$$\varepsilon_V = -\frac{1}{h}\sum_i \Delta h_i = \frac{1}{h}\sum_i \varepsilon_{V,i} h_i = \sigma_V \frac{1}{h}\sum_i \frac{h_i}{E_i} \quad (2.28)$$

2.3.2. The subsidence compaction relationship " Geertsma's nucleus of strain model" [2] [8] [10] [11] [12]:

By definition, subsidence is the motion of a surface (in our context the earth's surface) downward with respect to a reference (usually datum of the sea-level), which means that subsidence is quantified by a unit of length.

In order to build a mathematical relationship between compaction and subsidence, it's necessary to understand how the reservoir's depletion induced compaction propagates through the overburden in order to form what we call a subsidence bowl. This interaction between the shrinking medium and the surrounding medium is estimated as well through the help of the theory of poroelasticity. There has been several discussions before about this subject, mainly highlighting its similarity with the thermoelasticity within the mathematical frame. From which, the approach named ***"nucleus of strain model"*** was presented by Geertsma in 1973.

The conceptualization of this model starts from the estimation of subsidence from a compaction of a unit volume (e.g. a sphere), and to calculate the total subsidence of any assembly of small volumes, with the assumption that superposition of effects is admissible.

The technique is to consider the volumetric strain of the unit volume due to a pressure drop as a center of compression that induces a displacement field at the surface within the elastic domain. The displacements are determined by adding the contributions of unit volumes under the assumption of the linear elasticity of the whole depleting volume and its surroundings.

It's better described with spherical coordinates and their general solution for the displacement equation, if we consider a depleting sphere of a radius R_0 inducing a radial displacement at the surface u_0 , therefore the radial displacement at any distance r from the center of the sphere is given by the following equation Eq. (2.29):

$$u(r) = u_0 \frac{R_0^2}{r^2} \quad (2.29)$$

$\boldsymbol{u_0}$ ***:*** Radial displacement at the surface of the unit sphere.
$\boldsymbol{R_0}$***:*** Radius of the sphere.
r: distance from the center of the sphere.

By taking into account the relation between the volume change of the depleted sphere and the surface displacement, and the definition of volumetric strain we will end up with this resulting equation Eq. (2.30):

$$u(r) = -\frac{C_m}{4\pi} V\alpha\Delta P_f \frac{1}{r^2} \tag{2.30}$$

The final equation Eq. (2.30) is an indication that any subsidence is primarily proportional to the reservoir's compaction $C_m\alpha\Delta P_f$ while it entails as well the governance of the product of the reservoir volume and the pressure drop$V\Delta P_f$.

The inherent issue with such process is that it doesn't represent appropriately the surface at which the vertical load is null. The solution considered around the compacting sphere is supposed to propagate further from it until it vanishes at infinity. However, such consideration isn't fulfilled at the surface and interfaces where the elastic parameters vary. Therefore, it's necessary to impose a boundary condition *"free surface effect",* to complement the solution around the center. This problem was solved by analogy with provided solutions in thermoelectricity, implementing a vector expression Eq. (2.30) at the surface (z=0,$\sigma_z = 0$) Fig. 2.10 that corrects the general solution Eq. (2.31) given before.

$$\vec{u} = \frac{C_m}{4\pi}\left(\frac{\vec{R}_1}{R_1^3} + (3-4\nu)\frac{\vec{R}_2}{R_2^3} - \frac{6z(z+D)\vec{R}_2}{R_2^5} + \frac{2\hat{z}}{R_2^3}[(3-4\nu)(z+D)-z]\right)V\alpha\Delta P_f \tag{2.31}$$

For z=0, the solution becomes as indicated below Eq. (2.32):

$$u = \frac{C_m(1-\nu)}{\pi} V\,\Delta P_f \frac{1}{r^2} \tag{2.32}$$

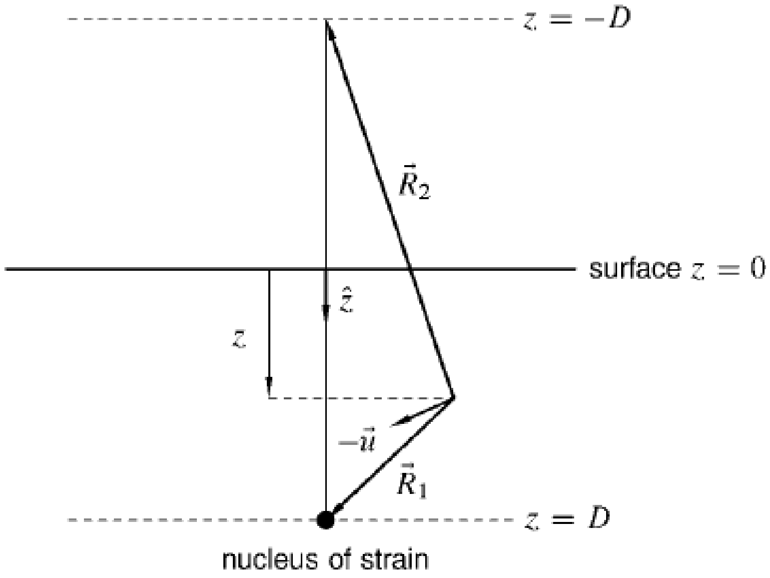

Fig. 2.10: Geometry for the Geertsma Solution. $\hat{\boldsymbol{z}}$ is the unit vector in the –z direction, $\vec{\boldsymbol{u}}$ indicates the direction of the particle movement for subsidence [2].

By integrating the vertical deformation Eq. (2.31) along the overburden over the entire surface, it's possible to estimate the size of the subsidence bowl, the resulting formulation Eq. (2.32) is [2]:

$$\Delta V_{subs} = 2(1 - \nu)\Delta V_{comp} \tag{2.32}$$

Geertsma's model is limited to the case where there is a negligible elastic contrast between the shrinking formation and its surroundings.

The nucleus strain model up to this point, didn't focus on the vertical uniaxial compaction, but was more general in terms of the direction of displacement. To circumvent such problem, it's possible to confine the compaction-induced displacement to only the overburden, while imposing no-lateral movement conditions. By doing so, it's possible to expect some up-word displacement by the rock under the reservoir. Literature is abundant with formulas that cater to such problems that are mainly shape dependent. In addition, we can find different models based on Geertsma's solution, estimating the subsidence of reservoirs with different shapes and mechanical properties, and situations where arching is present.

This traditional analytical method for the subsidence, has put forward an inherent issue in the reliability of the solution that is based on many simplifying assumptions. When in reality, reservoirs are the result of complex geological process, rendering the geomechanical volumes very inhomogeneous. In addition due to the properties contrast of the reservoir and its surroundings, the reservoir itself sometimes has to be divided into compartments to easily reproduce its possible diverse properties. Analytical solutions, can be flexible, time optimal and may provide decent results. However, for a reliable analysis, refined models are required to account for the considered volume complexities. Numerical methods are deemed more qualified for these advanced demands.

2.4.Geomechanical Modeling considerations:

The study of hydrocarbons production includes two main mechanically linked physical aspects: the rock medium and the fluid(s) contained in its pores. The mechanical effects induced by such production may modify the performance of said reservoir and can generate environmental alterations of its surroundings, caused by reservoir compaction and subsequent surface subsidence.

To assess the physical consequences of hydrocarbon production, several approaches have been proposed to couple geomechanical effects with subsurface flow, they were applied on several case studies of field applications providing us with comprehensive tools for a better understanding of recovery mechanics, stress field evolution, and production induced rock deformation and their effects on reservoir properties such as permeability and pore compressibility.

The challenge presented in the execution of a coupled analysis of multiphase flow simulation and stress analysis inside a routine petroleum engineering workflow is mainly the computation effort and time required for a full-field 3D simulation, especially that a geomechanical model can be significantly larger than a reservoir model.

2.4.1. Reservoir Dynamic simulation:

A proper representative dynamic reservoir model is one that can correctly estimate the bearing formation behavior during production while providing the ability to encompass the production induced effects on said medium, in this case geomechanical effects.

Reservoir flow modeling includes two complementary components [13]:

- ***A functional model*:** a set of differential equations and of numerical methods for solving equations.
- ***A representation model:*** mathematically describes the considered reservoir (rock and fluid properties) denoted through specific spatial variable coefficients, initial and final boundary conditions.

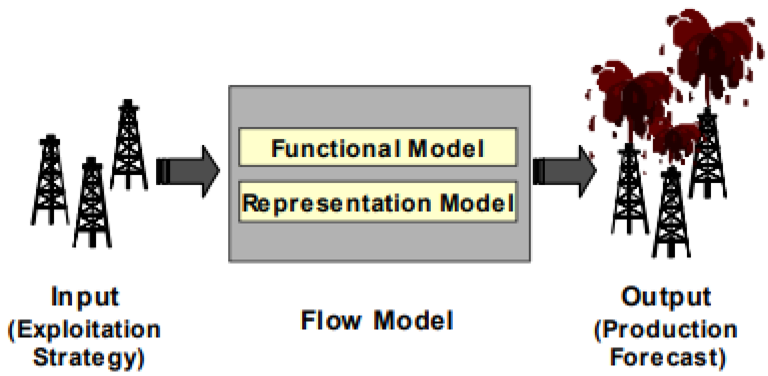

Fig. 2.11: Schematics of reservoir flow model components: the functional model and the representation model [13].

A full-scale representation of the reservoir (rock properties, fluid properties and their interactions properties) and production inputs are the main inputs for the dynamic simulation.

After calibration, the productivity and recovery forecasts are performed describing the reservoir's response to the imposed input parameters.

2.4.2. From dynamic flow to mechanical simulation:

Most classic commercial softwares/methods provide the option for the exclusive possibility for the fluid dynamic behavior to be simulated. This can be conceptually correct if certain model parameters (mainly permeability and porosity) remained constant (or underwent negligible variations) as the pressure depletion continues to alter the state of the stress of the reservoir and its surroundings. In due course, mechanical disturbances due to production are always present even if their effects are negligible on fluid extraction. Consequently, this allows a different array of Numerical approaches and computational scales to be used between dynamic flow and mechanical simulations.

Considering that the porous media is mechanically linked to its non-producing surroundings, and that its behavior is responsive to different conditions other than pressure drops with respect to its mechanical deformations. In addition to our focus on surface subsidence, it becomes necessary to extend the numerical Grid to include neighbor formations. into additional blocks [2] [14]:

- ***The overburden***: representing the rocks/soil lithology lying between the reservoir and the surface (seabed in our case). Its geometry, thickness and constitutive (mechanical) properties are introduced to ensure an accurate computation of the transmission of reservoir compaction effects into the surface.
- ***The sideburden***: it's the rock/soil adjacent to the producing zone. The sideburden has a great impact on the reservoir's stress path, in certain cases, for a "stiff sideburden"; during depletion the vertical stress can be transferred laterally instead of being completely carried by the producing medium "arching effects", emphasizing the need for an overall stress assessment.
- ***The underbuden***: it represents the rock underlying both the reservoir and the sideburden. The underbuden's degree of stiffness impacts the arching effect and stress distribution over the sideburden, as well as the the volumetric compaction of the reservoir as it correlates to the latter's stress path [2].

2.4.3. Coupling Strategies [15] [16] [17] [18] [19] [20] [21] [22]:

We can numerous papers and publications providing different technical and computational approaches on how to couple fluid-dynamics (reservoir simulation) with the geomechanical behavior of the reservoir and its surroundings. This is done to account for the interaction between mechanical deformation and fluid flow, where pressure and temperature distribution estimated by the reservoir simulator are fed to the geomechanical simulator. Once the stresses and the strains are calculated, they are passed back to the reservoir simulator in order to update the coupled parameters (porosity and permeability). From which, we can classify these techniques into different coupling levels depending on the code used for simulation. In its basic form, all coupled problems in finite element setting follow this general matrix formula Eq. (2.32) (Lewis and Schrefler 1987) [15]:

$$\begin{bmatrix} [K] & L \\ [L]^T & E \end{bmatrix} \begin{bmatrix} \Delta_t \vec{\delta} \\ \Delta_t \vec{P} \end{bmatrix} = \begin{bmatrix} \vec{F} \\ \vec{R} \end{bmatrix} \tag{2.32}$$

$[\boldsymbol{K}]$ ***:*** Stiffness matrix.

$[\boldsymbol{E}]$**:** Flow matrix.

$[\boldsymbol{L}]$***:*** Coupling matrix between the mechanical and flow unknowns (i.e. displacements and pore pressure).

$\vec{\boldsymbol{F}}$***:*** Vector of force boundary conditions.

$\vec{\boldsymbol{R}}$***:*** Residual of the flow equations.

$\vec{\boldsymbol{\delta}}$***:*** Vector of displacements.

$\vec{\boldsymbol{P}}$***:*** Vector of the reservoir's unknowns (Pressures, saturations, and temperatures)

Δ_t**:** Variation per time step.

2.4.3.1. Uncoupled approach [20]:

A conventional reservoir simulation where pore pressure distribution in space and time is estimated using fluid flow simulator, in which rock compressibility is the only mechanical parameter included in the flow simulation. Pore pressure changes are then added as input loads for the calculation of reservoir's compaction and subsequent subsidence. This method doesn't account for the pressure changes induced by variation of material properties (i.e. permeability and porosity variation) that are affected by depletion-induced stress variations. Meaning that petrophysical properties are assumed to stay constant over the lifetime of the hydrocarbon-bearing formation. In other terms, fluid-flow dynamics and stress-strain relationships are both solved independently Fig. 2.12.

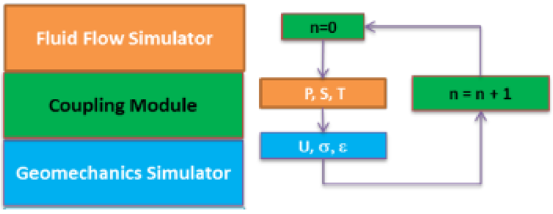

Fig. 2.12: One-way coupling approach.

2.4.3.2.Fully coupled approach [19] [20]:

This method solves simultaneously the flow and solid problems, as it calls to one integrated source code within the same grid and by adopting the same discretization. Its benefit is for it to provide a more likely accurate solution. However, such simulator requires a more complex computation and consequently it is more time consuming. Ideally this method can achieve a great representation of pressure distribution in stress-sensitive reservoirs.

2.4.3.3.Explicitly coupled approach [15] [20]:

An approach where there is a one-time step lag between the fluid-flow and the solid simulators. It will still solve each problem sequentially and separately, but in this situation the reservoir simulator will use the coupling terms porosity/permeability based on the geomechanical solution from the previous time step. This method provides an effective solution in simple depletion stress paths and is considered to be as rigorous as the fully coupled approach if iterated to full convergence Fig. 2.13.

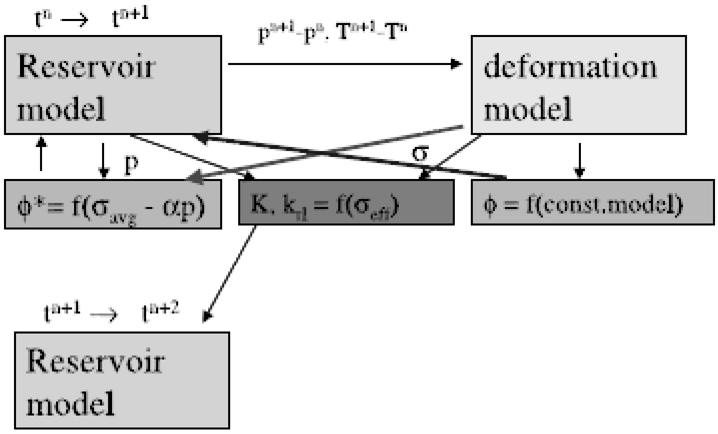

Fig. 2.13: Explicit coupling approach [20]

2.4.3.4.Iterative coupling [20]:

This method solves the two problems independently and sequentially, and then iterates the solutions within each time step until full convergence through the coupling module. Flow simulation assumes the stresses to be constant during each time step, rendering the unrealistic dependency of porosity to only pressure and temperature variations. While within the geomechanical solver, porosity is calculated by means of partial compressibilities that are function of pressure and temperatures variations in addition to the total stresses. The number of iterations is set by a convergence tolerance with respect to pressure/stress changes between two consecutive iterations. Such method allows the use of different simulators for fluid and mechanical problems and can be linked by means of a third-party iterative solver Fig. 2.14.

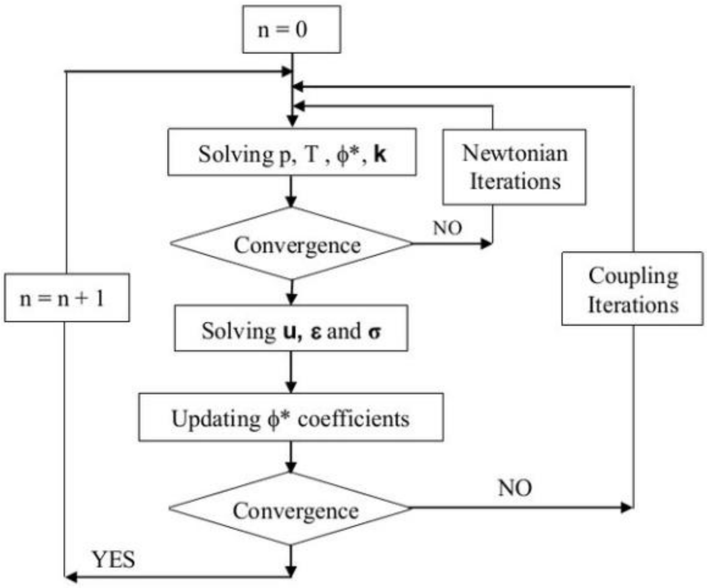

Fig. 2.14: Iterative coupling appraoch [22].

2.5.Numerical simulations:

The complex heterogeneous nature of petroleum systems coupled with the mathematical relationships describing their geomechanical behavior, calls for a higher degree of care in building a representative model to achieve accurate outputs. Undoubtedly, the quest for a detailed descriptive volume introduces severe computational challenges, urging engineers to continually improve solution methods or the establishment of new ones.

Analytical methods can provide insight over the mechanical behavior of the reservoir as well as the order of magnitude of the solution (compaction/subsidence), while numerical approaches are able to address aforementioned complexities through the use of powerful computational tools without having to over-simplify the problem. They approximate the solution over the whole domain within an expected acceptable error range. However, Numerical methods do not come without their own challenges, one of which their dependency on the accuracy of the input data.

We have focused our work scheme for the geomechanical response of the reservoir rock and its surrounding within the elastic domain. Therefore, the numerical methods treated, in this thesis, are designed to solve the considered elasticity problems. In The next subchapters, FEM and VEM will be shortly explained.

2.5.1. Finite Element Method:

Essentially every natural phenomenon biological, geological or mechanical can be expressed with the aid of the laws of physics. The mathematical formulation of these space- and/or time- dependent processes often results in statements expressed in Partial Differential Equations (PDEs) relating quantities we are interested in for the construction or perception of said physical processes. [23]

Finding a solution for PDEs through exact methods of analysis is a daunting task for the majority of geometries and problems. Preferably, numerical methods are used to calculate approximate solutions. Among these the Finite Element Method (FEM) is the most used in literature and is used in the commercial software that is partly subject to our study. [23]

‘’ .... The idea behind the finite element method is to break the spatial domain up into a number of simple geometric elements such as triangles or quadrilaterals. The weighted residual concept is then used to approximate the solution function over each finite element domain. Care needs to be taken to ensure continuity of the dependent variables and their first partials in moving from element to element. Partial differential equations are therefore transformed into sets of ordinary differential equations in time. The method is particularly suited for solving problems involving irregular geometries ...’’. [24]

2.5.1.1.FEM solution procedure:

From a phenomenon point of view the studied geomechanical problem can be synthesized as the forecast of the behavior of a system that is subjected to external loads that represents the disturbance to the state of the system. As mentioned in the introductory part of this subchapter, we are going to look for a numerical solution to the governing equations that characterize the behavior of the system [25].

In order to summarize the workflow of the Finite Element Method, I sought out to arrange it into few simplified steps, as follows [23] [25]:

1. ***Discretization of the continuum domain*:** the aim of this step is to discretize the geometrically complex domain of our problem into smaller regions (sub-domains) called finite elements with a “fixed” shape (i.e. tetrahedron or bricks). It is

important to mention that these elements don't overlap and they are interconnected, leaving no gaps, at a discrete number of nodes situated at the respective boundaries of each cell. Nodes of neighboring cells are coincident. Typically hanging nodes are not allowed. The resulting arrangement of the cell-node network is called a Mesh (grid).

2. ***Selection of the shape function on the reference element*****:** Shape functions approximate the solution (displacement) on each element. Their definition derives from the idea that continuous functions can be approximated by using linear combinations of algebraic polynomials (basis function). NB: the degree of polynomials depends on the number of nodes appointed to each element and the order of the differential equation being solved.

3. ***Construction of the element stiffness matrix*****:** the displacement of the nodal points are set to be the unknowns of the problem. Exploiting variational formulation and Galerkin approach a matrix equation is then formed linking nodal values of the unknown function of our problem to the other parameters.

4. ***Assembling of the global matrix*****:** All Local element equations with respect to each elements are combined to construct the Global Equation System. The latter defines the entire response of the system and its dimension depends on the number of nodes and degree of freedom of the problem.

Boundary conditions must be defined and then imposed before the next step. Which is usually done by modifying the system equations by adding values to existing terms and/or shifting the terms from one side to the other. [24]

5. ***Solution of global equation system*****:** The resulting algebraic system of equation is solved through conventional numerical methods (Direct or iterative). The solution can be given at each node and interpolated to the centroids by means of shape functions interpolations.
6. ***Computation of additional results*****:** other physical properties can be derived from the solution and displayed with respect to the problem and solution need at hand.

It is important to highlight that; this analysis can only provide an insight into the physical problem at hand. It's not feasible to predict the exact response of the system because it's not possible to reproduce even with the most refined model all the information present in nature and consequently implicated in the physical problem.

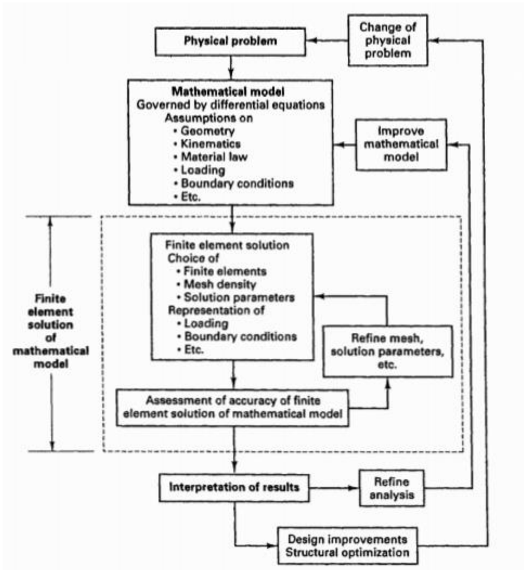

Fig. 2.15: The process of finite element analysis.

Through the years FEM has been established as the most reliable numerical mathematical method for solving engineering problems, and particularly geomechanical simulations. What allowed this method to stand out among others is: the independence of the algorithm to geometrical complexity of the domain, the straightforward fashion in enforcing natural and essential boundary conditions and most importantly a relative high-level solution accuracy depending on the provided computational effort. ***However, these beneficial features have a major drawback fostering strict rules on the mesh design construction*** [26].

These rules have a tendency to challenge the practicality for the solution of several complex problems in modern solid mechanics, specifically in the 3D domains, where a mechanical design of extremely complex components may require weeks of human effort to reproduce an adequate mesh [26].

Thus, the idea of introducing arbitrary polyhedral elements to provide much flexibility in the discretization of complex engineering domains. Rendering unstructured grids [3] attractive in the meshing of said complicated domains. [27]

Several approaches have been developed trying to extend the Finite Element Method to non-traditionally shaped elements such as general polygons, and polyhedra. Within this theoretical framework, the Mimetic Finite Difference Method[4] (MFD) has been proved over simple quadrilateral meshes for unstructured polyhedral meshes, while preserving the fundamental properties of the underlying physical and mathematical properties. [28] [29]

Among the different proposed numerical methods, the newly **V**irtual **E**lement **M**ethod comes to light, a method that is considered as an evolution of the Mimetic Finite Difference Method (MFD) diffused on problems with relatively irregular decompositions [29].

2.5.2. Virtual Element Method [28] [30] [31]:

For the trained eye, this new method can be easily identified as the ultimate progression of the Mimetic Finite difference approach. However, within the last step of VEM development, it has become clear that its implementation resembles more the Finite Element Method. In addition to the particularity of the VEM were the local shape functions of each element are defined implicitly which led to the use of the term “Virtual”, and the provision of a whole new perspective.

Fundamentally speaking, VEM shares the same spaces (domains) as FEM with additional suitable non-polynomial functions. The latter are harder to create or handle, which is why VEM operates in a way that allows the computation of the Matrix stiffness without having to actually compute these non-polynomial functions.

There are several aspects that favour VEM in comparison to other numerical methods:

- Its firm mathemtical foundation.

[3] Unstructured grid: A mesh identified by irregular connectivities.
[4] Mimetic Finite Difference Method: A numerical method that mimics fundamental properties of mathematical and physical systems, by creating discrete approximations that preserve the properties of the considered equations on general polygonal and polyhedral meshes [32].

- Its simplicity in implementation.
- Its accuracy and efficiency in computation.

This Procedure will allow us to easily manage complicated element geometries and/or higher order-continuity conditions. This broad conceptualization provided by the Virtual Element Method, allows the user to have a wide range of possibilities on how and where to exercise it on large scale of different engineering problems.

2.5.3. Finite Element and Virtual element discretization [24] [15] [14] [17] [18] [19] [20] [21] [33] [34] [35] [36] :

The geometric considerations to build a geomechanical model can be limiting in order to achieve an accurate solution. The advancement in the geophysical acquisition methods continually improves the understanding of sedimentary formations and their characterizations, allowing engineers to provide better interpretations of stratigraphic structure. In other terms, we have a better grasp on the spatial correlations contrast of spatially/directionally dependent parameters that can lead to distorted cells shapes or high aspect ratio cells during mesh generation phase.

Often, these complexities may lead to information losses when building a geomechanical mesh. Certain numerical methods are robust for these irregularities by inducting grid simplifications, yet this can prompt inaccurate system responses. Therefore, highly distorted elements not only effect computation time, but, if not dealt with, they will influence the final results as well.

It follows that the challenge lays in finding the optimal compromise between a representative geological structure and an adequate numerical method. Conventional commercial softwares solve the geomechanical problems using the finite element method. This method has shown a satisfactory level of flexibility in dealing with grids resulting from complex geology structures. Bearing in mind that the delta pressure map which represent the main loading term in reservoir geomechanical simulation comes from flow simulation which, in turn , it is performed independently using a different grid and a different numerical approach,typically Finite Differences Method on corner point gridding. In a traditional workflow the reservoir grid is extended to allow the estimation of production induced mechanical deformations. Such a step it is possible only if certain constraints are imposed mainly on shape functions[5], and yield[6] criteria for it to have an admissible global solution. Evidently, to exploit the corner point gridding inherited from flow simulation, FEM requires a specific type of cell shape “Hexahedron” formed by connecting adjacent pillars defined with a two dimensional Cartesian Partition. Several workflows were developed in order to generate suitable results for mechanical simulations, without having to excessively refine the mesh.

The literature supports the general consensus that Unstructured Meshes are the best representation of subsurface sedimentary sequences while respecting the physical parameters, and the complex structures of the system. Theoretically speaking, being able to manipulate this grid format is ideal for geomechanical applications. However, the compromise needed to run such computations, severely alters the solution.
Considering that VEM is an extension of FEM generalized over polyhedra, it will inherently adopt the properties of the standard method. This will allow engineers to bypass errors induced by structural simplifications, and overall meshing limitations imposed on standard grids used by simulators. In addition, to already having the path mapped out for an easier way to couple the multiphase model to the VEM geomechanical model.

[5] Shape function: The function which interpolates the solution between the discrete values at the grid nodes.
[6] Yield: On-set for plastic deformations.

3. Model building and Comparison Methodology

At this early stage of development, the scope of VEM applications is focused on case comparisons with the aim of validating the method against a FEM classical simulator and of integrating the solver in the traditional reservoir study workflow. The tested VEM code is developed by the GEOSCORE Group[7] in collaboration with the Petroleum Engineering Group[8]. At the present, the VEM solver doesn't offer the possibility for a complete geomechanical modelling setup. Therefore, parallel channels are considered to circumvent this issue. Details will be further disclosed in this chapter.

The Finite Element Geomechanical solver used for the benchmark is VISAGE[9] which is integrated in the Petrel E&P platform by Schlumberger with the name of Petrel Geomechanics. Petrel provides a graphical interface to accommodate the support needed by the VISAGE simulator for data configuration and solution visualization. Petrel Geomechanics provides a self-contained workflow, enabling the 3D/4D modeling of rock stresses and deformations in reservoirs and their surroundings. This includes pre-processing, model creation, property modeling, simulation-launch and case management, in addition to post processing, results analysis and visualization.

The dynamic reservoir simulations are performed by the commercial software ECLIPSE, considered as an industry-reference reservoir simulator. The simulator is used to calibrate the reservoir model and forecast its dynamic flow behavior. The software can be accessed independently by use of a launcher or can be accessed through the Petrel E&P platform.

Advantages of the Petrel E&P platform is the integration of multiple disciplines, user friendly standardized workflows and multiple file format data storage. The Workflows are optimized in a manner which allows straightforward data testing and scenario analysis. In particular the standardized workflow from model building to solution visualization for the compaction (induced by depletion) and the subsequent subsidence will be described accordingly.

[7] DISMA: Department of Mathematical Sciences.
[8] DIATI: Department of Environment, Land and Infrastructure Engineering.
[9] VISAGE: Vectorial Implementation of Structural Analysis and Geotechnical Engineering [37].

Starting from Petrel we arranged parallel workflow (mainly by Matlab scripts) to process the data in order to prepare the input model for the VEM simulation.

At the basis of the geomechanical model construction, there is the definition of the 3D static model which derives from a geological study which integrates lithological and petrophysical characteristics within the grid (layers, anticlines, pinchouts…etc). Properties are assigned to each grid block with respect to the purpose of the simulation. The reservoir zones are populated by petrophysical properties fluid saturations, porosities as the main parameters regulating the original hydrocarbons in place; and permeabilites controlling the ease at which the fluids flow within the reservoir. Modeling is performed at reservoir scale and then extended to the regional one in order to capture the full mechanical response of reservoir depletion while assuring that the boundary conditions do not affect the computed solution.

3.1.Dynamic reservoir simulation:

The objective of this step is to simulate the dynamic flow behavior of the considered reservoir in order to create realistic scenarios to test the VEM against FEM solution.

Components of a dynamic reservoir model we considered are [17]:

- The static model.
- Rock, fluid and rock-fluid interactions properties.
- Equilibration data (i.e. initial conditions).
- Productions scenarios.

In particular, once the reservoir model is built, discretized and populated, we proceed to the initialization process, through the assignment of initial fluid saturations, pressure distributions (datum depth, datum pressure and fluid contacts were fixed). Objective of this phase is to meet the original hydrocarbons in place provided by eclipse with respect to the one provided by static modelling.

During simulation phase, the input parameters are tuned to achieve a range of pressure depletion high enough in order to get an acceptable induced subsidence respect to the solution discrepancy of the two solvers.

When preparing scenarios our main focus is directed towards the parameters affecting the dynamic flow behavior, more precisely absolute permeability and porosity. The dynamic simulation was run independently via an Eclipse launcher. To easily handle porosity and absolute permeability maps, we import the Eclipse dataset and simulation results to the Petrel E&P platform, for a more practical manipulation of pressure, porosity and permeability as model properties.

3.2.Geomechanical modeling:

The steps followed for Model setup are accommodated via the Petrel Geomechanics interface. As emphasized before, geomechanical analysis is performed primarily for safety analysis on a regional scale, to account for stress-strain variation effects on the reservoir and its surroundings. So, the first step is to increase the volume of investigation through grid extension to capture the full geomechanical response due to reservoir production, along with making sure that boundary conditions do not affect the computed solution. Usually the reservoir is positioned roughly in the middle of the simulated volume.

The extension is achieved by providing a representative lithological sequencing of the field or the basin we are modeling. Conjointly, we choose the discretization strategy. Because the number of cells influences the simulation time, we sought out to refine only the areas of interest. Therefore, the scope of focus is towards the reservoir region and the area directly above it "The overburden". Inversely, all regions exhibiting negligible or null stress-strain changes due to production are discretized by coarse gridding. It is observed that the absence of aquifers makes the area affected by the subsidence rather limited.

After the incorporation of the geological characteristics within the considered volume, we assign each stratigraphic section the appropriate mechanical parameters: elasto/plastic moduli, rock strength, and density. The values are assigned to each cell within the grid.

We established that the model's solution is sensitive to the coupling degree between the dynamic fluid-flow problem and stress-strain problems. The reason behind our choice selection will be explained in the next chapter. At the same time, we set up the initial pressure profile of the reservoir, as well as, the static pressure evolution resulting from the reservoir's imposed production history which comes from the dynamic reservoir simulation (ECLIPE's solution).The platform allows to manipulate the pressure as a model property, by storing its evolution as independent properties with respect to different time-steps. At this stage we consider only the full reservoir-imposed depletion, thus by introducing the initial reservoir pressure profile and the final one after production, in order to have an overall stress-strain evolution pertaining to surface subsidence.

To run a geomechanical simulation, stress distribution over the full volume is required. This phase is performed by imposing a hydrostatic pressure regime and estimating a vertical stress profile through a looping workflow which incrementally take account of the contribution of overhead layers by adding contribution to lithostatic pressure of each cell.

Petrel Geomechanics, offers a variety of output selection. In the context of our thesis, the main outputs are displacements, strains, stresses and Pore-pressure.

Up to this point, we have detailed the steps followed to prepare a geomechanical model within the integrated frame of the Petrel E&P platform. This self-contained workflow doesn't expose the user directly to VISAGE. However, once the simulation case is ready for simulation, it's implicitly passed to VISAGE for Finite Element numerical stress-strain computations, and then Petrel Geomechanics uploads the results for analysis and data visualization.

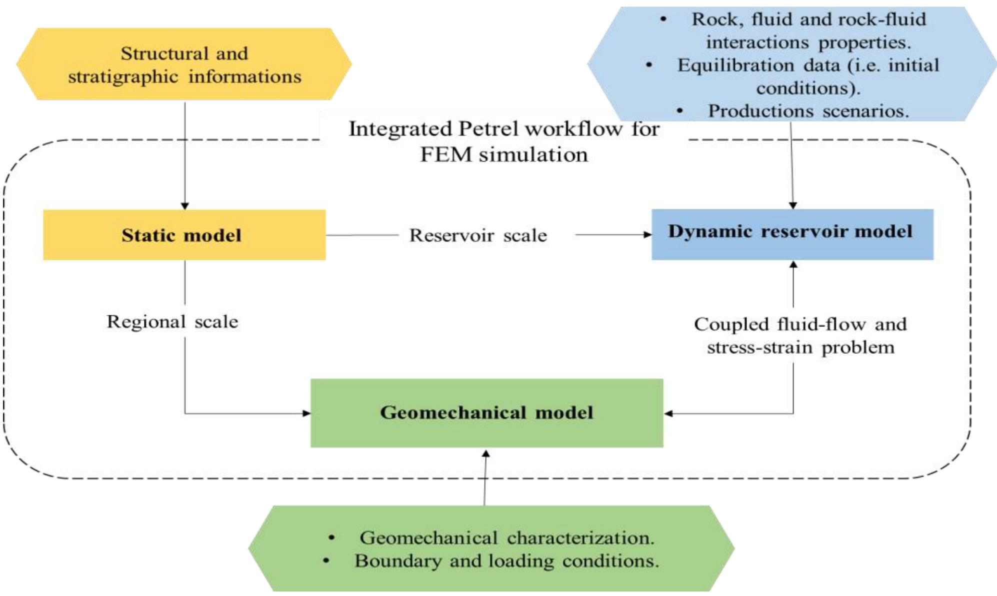

Fig. 3.1: Integrated Petrel workflow for FEM simulation [21].

3.2.1. Lack of Graphical Interface User for VEM:

First objective was to import the model from Petrel Geomechanics in the VEM code. For this specific task, a dedicated Matlab code is developed to populate the VEM model.

We exploit the option offered by Petrel to export data into files, in order to be managed by third party softwares. The properties that need to be exported are: grid geometry, mechanical properties, and pressure profiles at the reservoir scale resulting from an imposed reservoir production, densities and a boolean property the net gross which is used for the identification of reservoir cells.

We export the aforementioned properties as .GRDECL[10] files. This format allows the export of the corner point grid defined in Petrel (structured), and to store the exported properties as cell data.

It is observed that .GRDECL is built to manage structured grids. Ergo, the necessity to convert our files into a more flexible configuration to handle the VTK unstructured mesh which represents the standard input of the tested VEM code. A Matlab script was written to convert the Petrel structured grid format to a .VTK[11] file..

VTK unstructured grid object is able to support a wide range of datasets of arbitrary cell configurations and types, as opposed to regular GREDECL files which is limited to hexahedron. The VTK syntax organizes the definition of the grid by nodes, cells and cell types. In order to manage the irregularity of the meshes, the nodes are referenced by ID-numbers, while the cell are supplied by a number of faces and an ordered list of nodes that define it [38].

Once the model is set up, the VEM mechanical simulation can be run.

[10] GRDECL: "GRID ECLIPSE" is a file format that stores the properties in hexahedral cells which define the geometry of the field.
[11] VTK: Visulization ToolKit.

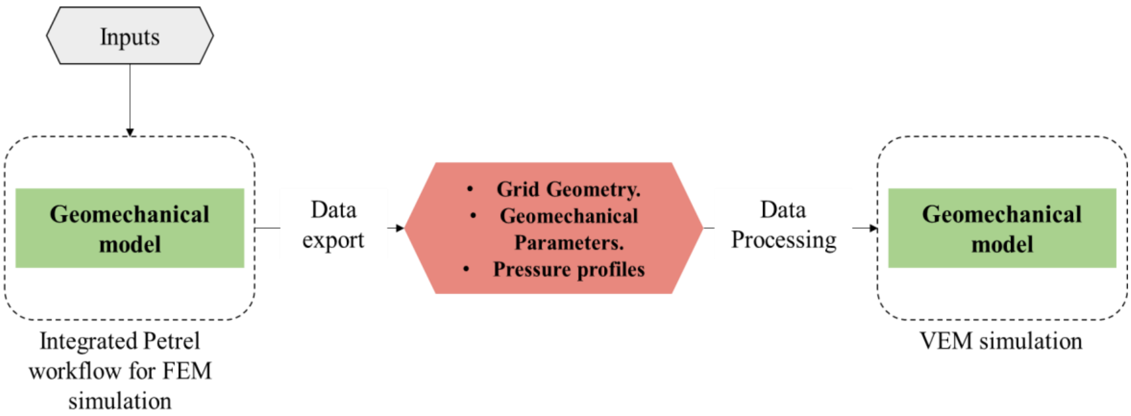

Fig. 3.2: Model building for VEM simulation.

3.3.Setup for comparison process using a third-party software:

In order to analyze the solutions obtained through two different simulators on the same grid, it's necessary to construct a workflow that allows both a qualitative and a quantitative comparison.

Petrel interface provides the possibility to manipulate the input data and analyze the results obtained from its integrated FEM geomechanical simulator. However, coherently with the modelling approach implemented in the whole platform, properties are associated to the cells, thus node displacements and stress obtained from FEM simulations are processed and someway interpolated to the centroids of the grid cells. Consequently, we can't directly compare FEM original results to the VEM ones through this interface. Hence, the necessity to introduce a third-party software that provides the necessary visualization tool to perform comparisons.

To this task, we employ ParaView[12]. This tool is able to process a large number of datasets including unstructured meshes. It is not by chance that the VEM solver input files respect the VTK syntax. Evidently, to close the loop we have to export the inputs/outputs of FEM simulations and convert them into a dataset that ParaView can process

[12] Paraview: an open source application for visualizing two- and three- dimensional data sets based on .VTK libraries.

3.3.1. Qualitative comparison:

For a qualitative comparison, it is sufficient to consider the solution associated to the grid elements. Therefore, we will export input and simulations results data from Petrel using the proprietary GRDECL format which lists the grid geometry and the properties associated to each cell. The already mentioned Matlab script is employed to handle the conversion to a VTK file read by the ParaView application.

3.3.2. Quantitative comparison:

By definition, FEM calculates the solution at node positions, thus it can be derived in correspondence of the centroid of each element, for example by means of geometric or arithmetic averaging, depending on the type and order of the finite element that is used. Petrel exports the centroid based solution to the user interface which provides the visual support to analyze the mechanical deformations induced by production (compaction and subsidence). However, for a more accurate comparison between FEM and VEM solution, it's necessary to conduct the analysis at node positions.

For the purpose of acquiring the FEM nodal solution, it's possible to call VISAGE directly and bypassing Petrel by the means of ***batch processing***[13]. This method allows us to collect and process data through a series of executable commands in a script, where it is also specified which and where inputs/outputs should be stored.

By this way of setting and launching FEM simulation, it was possible to explicitly save the nodal solution instead of element one. Moreover, in order to limit the dimension of the output file, it was possible to list the output parameters, in this specific case: displacements, stresses, pressure differences and constraints. In addition, the setup of the batch run requires grid topology, nodes coordinates, nodal constraints for each simulation step, initialized cell stress and pressure, and cell pressure variation. All data are exported from Petrel in a dedicated folder where a collection of files is stored. Among input information, they also contain batch processing commands to run the FEM simulation. Simulation results are then stored in a dedicated file and thus compared with the VEM nodal solution (readily provided by the simulator).

[13] Batch processing: a form of data processing in which a number of input commands are grouped for processing during the same simulation run.

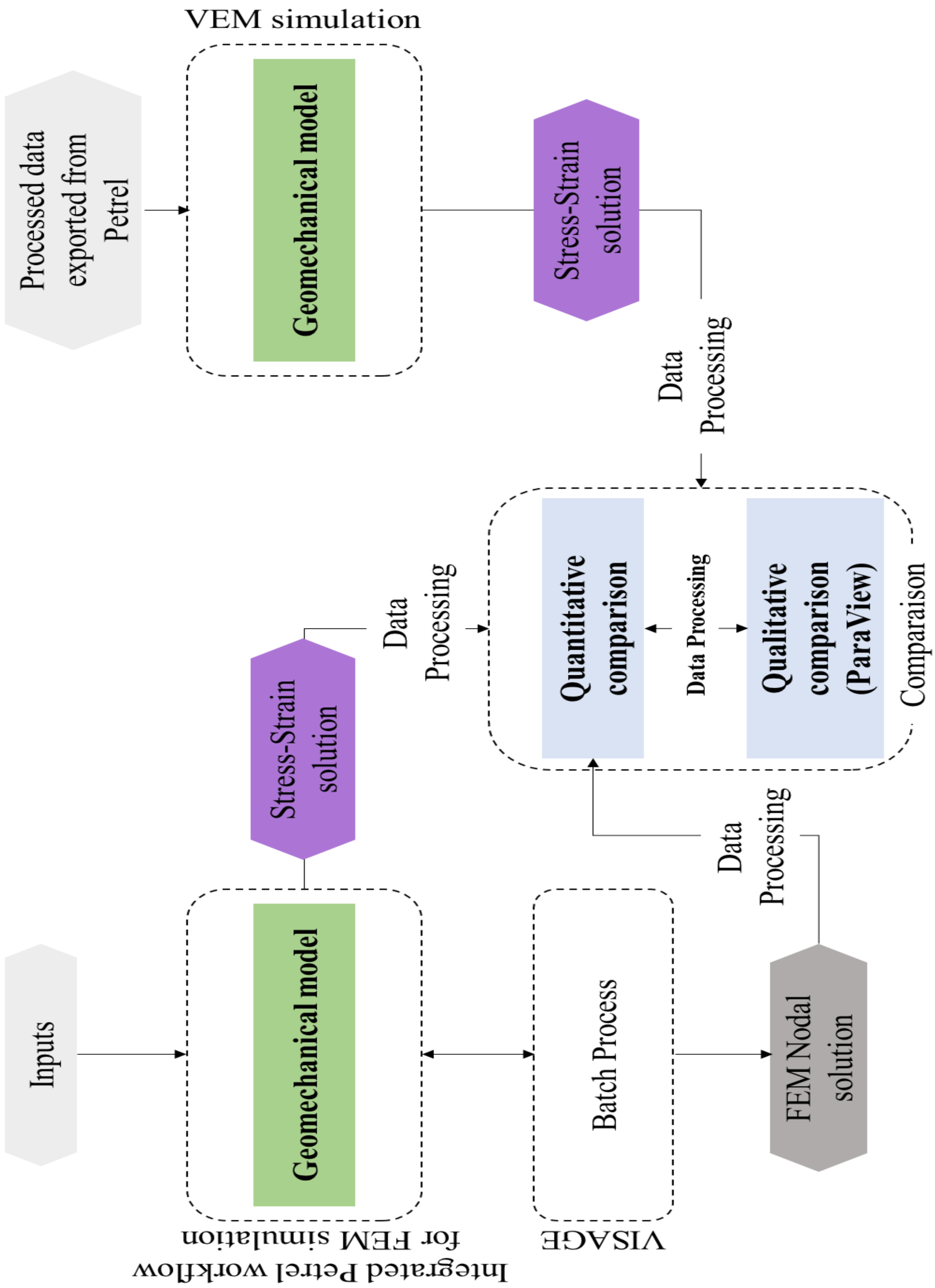

Fig. 3.3: Workflow for comparison process of the FEM and VEM Geomechanical simulations.

4. Numerical test cases

4.1. Case study 0:

The first case study is a synthetic simplified isotropic homogeneous elastic model built primarily to reduce as numerically as achievable the possible sources that can induce solution discrepancies between the FEM and VEM simulations.

As mentioned before, the reservoir simulator allows non-flow units such as in the case of presence of faults, impermeable layers... etc. When the Eclipse solution is passed to the extended geomechanical module, stored as cell properties, it will be translated as discontinuous pressure distribution between two adjacent cells (and more precisely at the concerned possible boundary) within the extended mechanical mesh.

The geomechanical simulators FEM/VEM require the pressure terms to be defined at the node and consequently at the boundaries, which is done by extrapolating the pressure from the element centroids to the element nodes. However, for confidentiality reasons we cannot recreate the same method for pressure discontinuities handling and the same method for data extrapolation used by FEM simulator VISAGE over the VEM code.

Additionally, the VEM code used for simulation imposes a no displacement conditions at the boundary for all three directions, as opposed to VISAGE which imposes a no displacement condition only at the plane that is perpendicular to one coordinate axis, as for the remaining two coordinate directions the used boundary conditions to close the loop remain inaccessible.

As a starting point, to mitigate these possible sources for solution discrepancy between the two simulators, we have considered these steps:

- We adopted a simplified grid geometry for both the source of pressure depletion and the extended geomechanical volume. It is a regular structured grid, with standard hexahedron cells.

- To reduce the effect of data extrapolation on the last results, we have considered two mitigation paths utilized simultaneously:

Constant Geomechanical parameters Tab. 4.1: the considered volume is homogenous over the whole domain, in order to eliminate the possible cause of discrepancy due to the input elastic moduli and the mechanical parameters extrapolation. A constant distribution of these parameters is then constant over the nodes for both simulators over the whole solution domain.

Tab. 4.1: Mechanical properties of the synthetic model Case 0.

Parameter	
Bulk Density ρ (kg/m^3)	2000
Young modulus E (Gpa)	3
Poisson ratio υ (-)	0.35
Lamé's coefficient λ (Gpa)	2.592
Shear modulus G (GPa)	1.111

Pressure distribution approximation Fig. 4.1: a source of pressure depletion was prepared analytically where the maximum pressure drop is at the center of a parallelepipedal volume with dimensions x×y×z (600m×600m×600m), while it decreases continuously away from the center until it becomes null at its boundaries. The pressure decline over the volume is given as a discrete drop of delta pressure steps expressed at the centroids of each cell. In addition, the smooth decrease is adopted in order to reduce as much as the possible the discrepancy of delta pressure distribution between the cells and consequently between the nodes. At the boundary of source of pressure depletion, the pressure is null, in order to avoid the discrepancy that can be caused by no-flow boundary when extrapolating pressures.

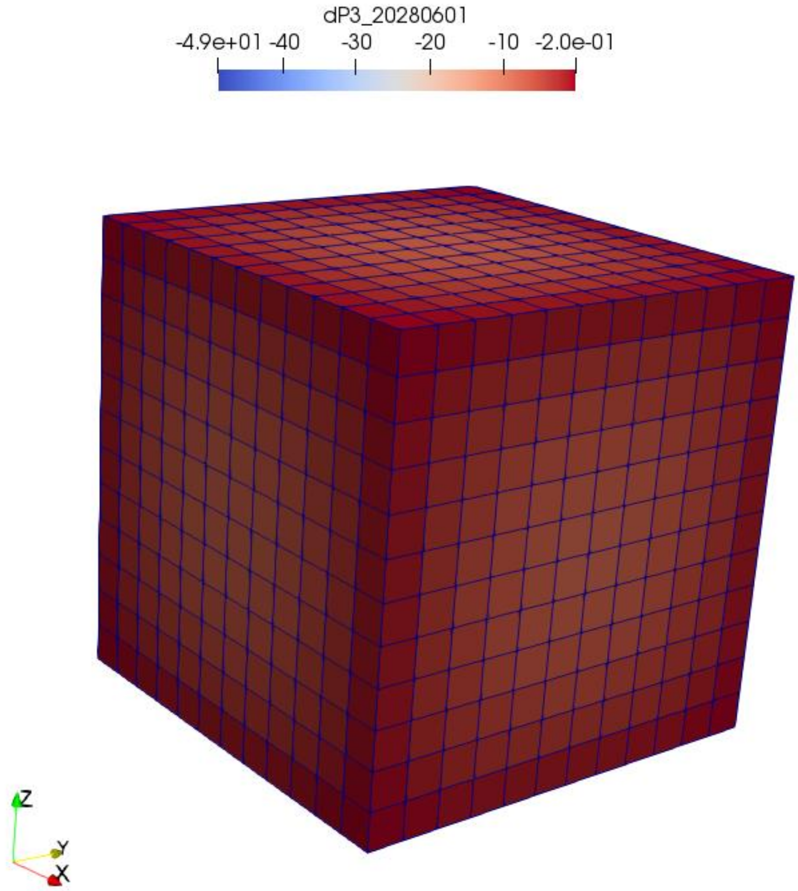

Fig. 4.1: Delta-Pressure distribution [bars] at the level of source of where the displacement field is nI×nJ×nK (12×12×12) (Paraview visualization).

- In order to assess the possible impact of the different boundary conditions used by both simlators on the solution approximation of the induced displacement field, we tested two geomechanical volumes which differ for vertical extension (z direction) Fig. 4.2. Concequently, the first grid's underburden was extended beyond the dispalcement field x×y×z (10000m×10000m×6500m), while the second grid's vertical extension was reduced in order to interfere with the solution x×y×z (10000m×10000m×3500m).

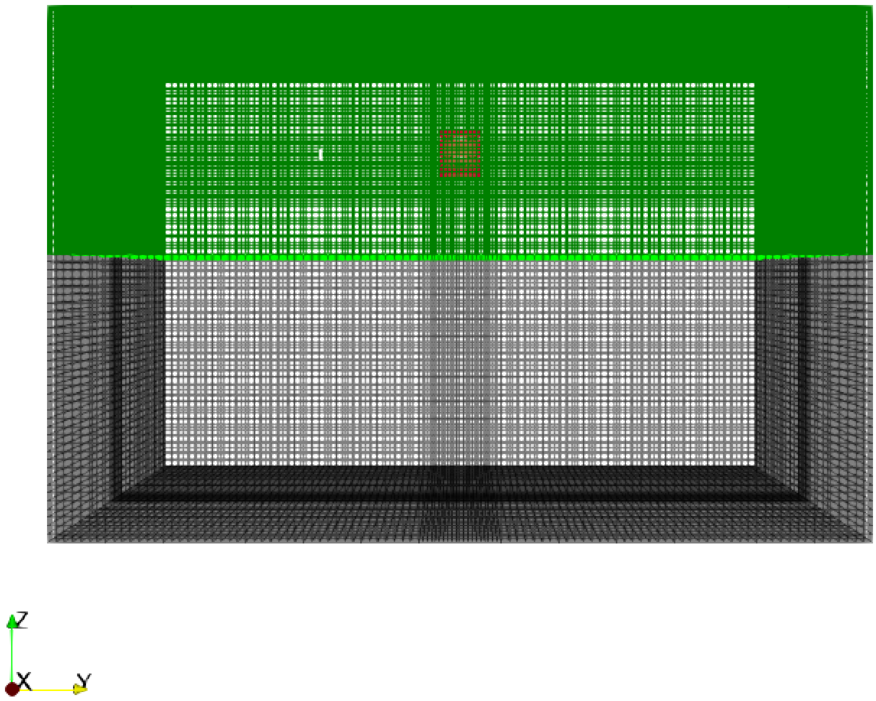

Fig. 4.2: The geomechanical grids of case 0 (Paraview visualization):
a) red grid: source of pressure depletion, b) green grid: geomechanical volume of non-extended model, c) green+grey grid: geomechanical volume of the extended model.

The processing and comparison workflow described in the third chapter was then applied on the two considered geomechanical volumes.

4.1.1. Results and discussion:

The performance of VEM and FEM simulations in terms of vertical displacements for the non-extended and the extended are shown below Figs. 4.3 to 4.6 and Tab. 4.2:

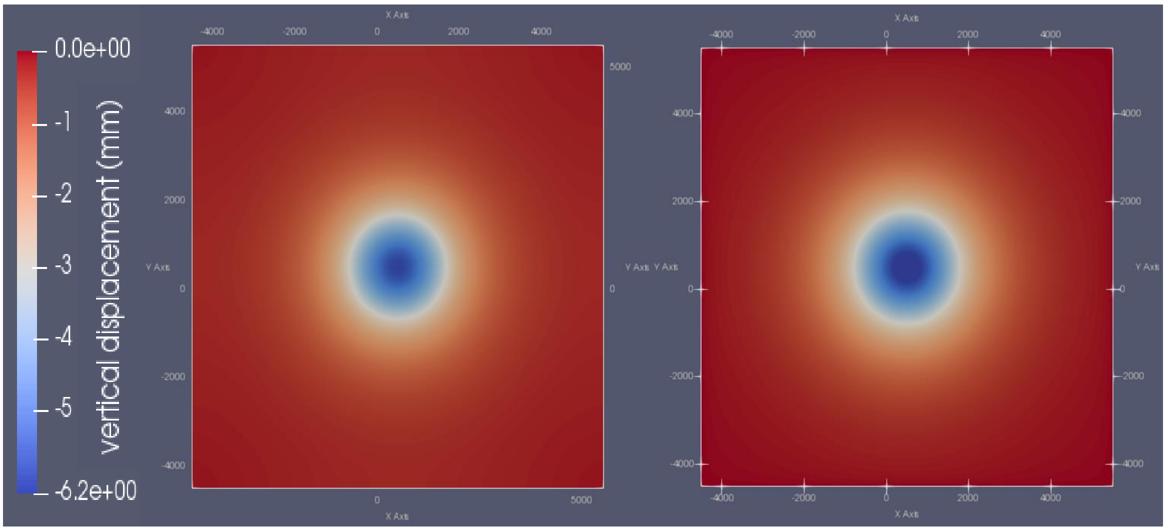

Fig. 4.3: Top view of the approximated subsidence (displacements along the z-axis) on the non-extended grid: VEM solution to the right, and FEM solution to the left (ParaView visualization).

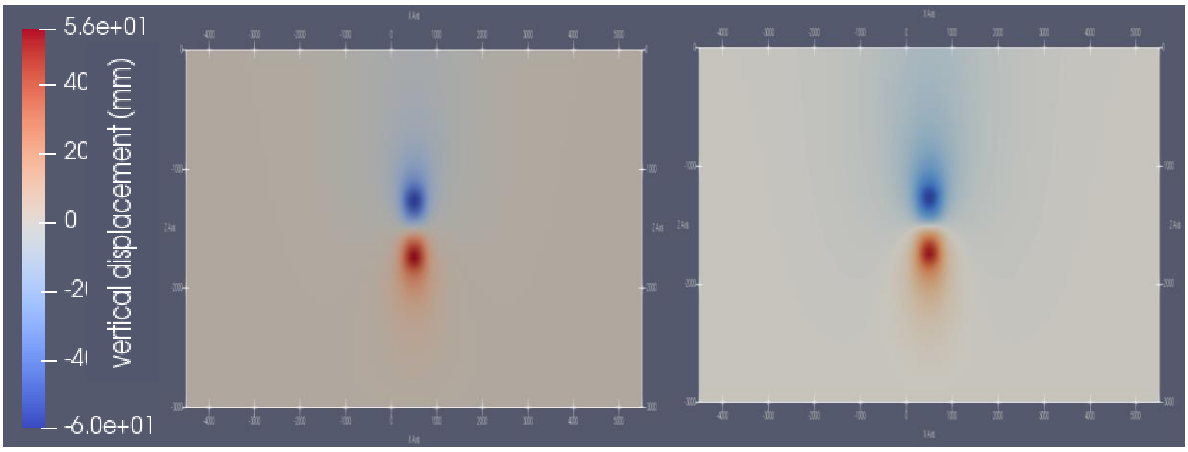

Fig. 4.4: Vertical section approximated subsidence (displacements along the z-axis) on the non-extended grid: VEM solution to the right, and FEM solution to the left (ParaView visualization).

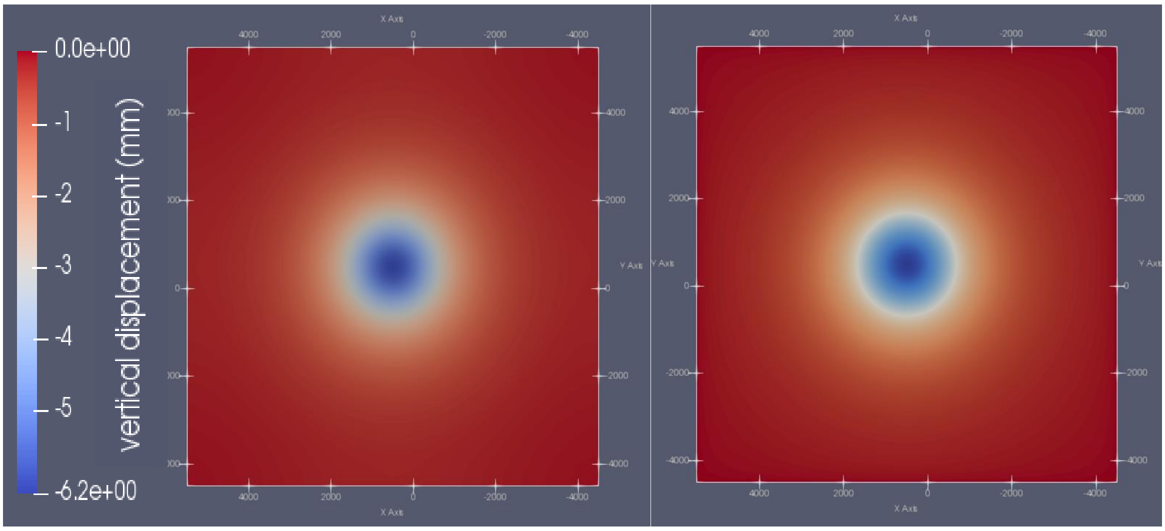

Fig. 4.5: Top view of the approximated subsidence (displacements along the z-axis) on the extended grid: VEM solution to the right, and FEM solution to the left (ParaView visualization).

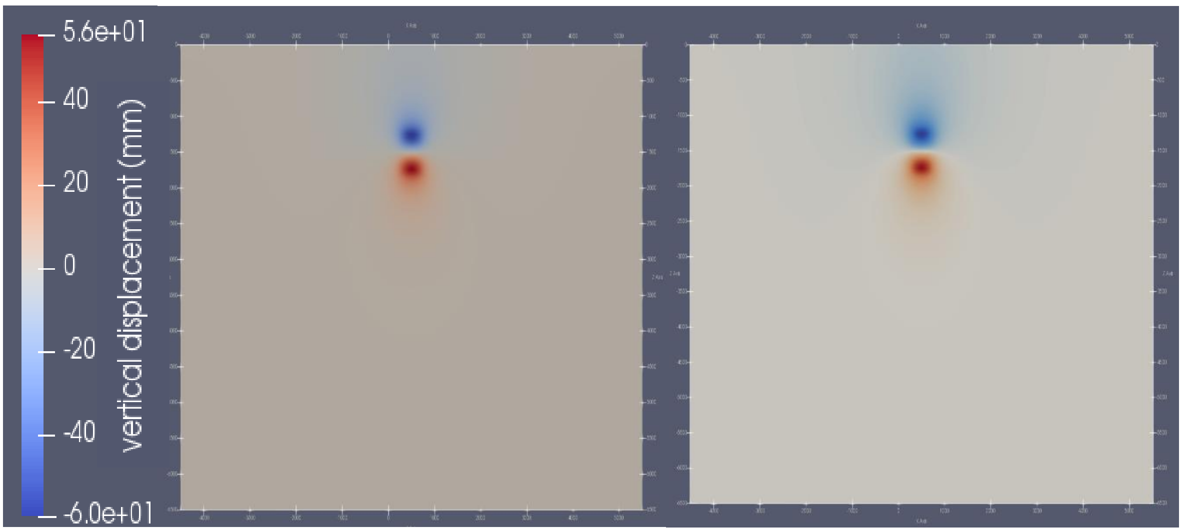

Fig. 4.6: Vertical section approximated subsidence (displacements along the z-axis) on the extended grid: VEM solution to the right, and FEM solution to the left (ParaView visualization).

Tab. 4.2: Summary of Calculated displacements of FEM and VEM solution (case 0)

	Non- Extended grid		**Extended grid**	
	FEM	VEM	FEM	VEM
Maximum displacement at the surface (subsidence) in mm	-6.08385	-6.63764	-6.0945	-6.17129
Maximum displacement over the whole volume in mm	-59.9485	-59.7333	-59.8883	-59.0659

In Figs 4.4 and 4.6, we can observe that the source of pressure depletion undergoes an uploading (in red) and a downloading (in blue) that extends within the pressure volume until it cancels out at the center. The behavior is due to the continuous delta pressure variation within the source volume. At the center, the cells, having the highest delta pressure as a loading factor, induce the highest displacement field around it. The adjacent cells, having a lower delta pressure, will generate a relatively weaker displacement field than the center. By, considering the superposition of displacements, we will observe a concentration of displacements downwards and upwards towards the center where they cancel out.

Qualitatively, the numerical solutions obtained by the VEM code seem to reliably simulate the phenomena in terms of magnitude of displacements and the extension of the solution over a regular hexahedron grid. In both grid-extension scenarios, the VEM approximation gives much appreciated results with a difference in the order of magnitude from 10^{-1}millimeters to millimeters.

To evaluate the discrepancy of solution approximation of VEM, we compare the solution at each node of the grid, by calculating the absolute norm relative error Eq. (4.1) in displacements between VEM and FEM with respect to the maximum displacement estimated by FEM. The calculations are done for each grid independently.

$$e_{rel_i}[\%] = \frac{|dz_i^{FEM} - dz_i^{VEM}|}{\max \_dz^{FEM}} \times 100 \tag{4.1}$$

i: node ID.

In Figs 4.7 and 4.8, we show the error evolution over the solution domain.

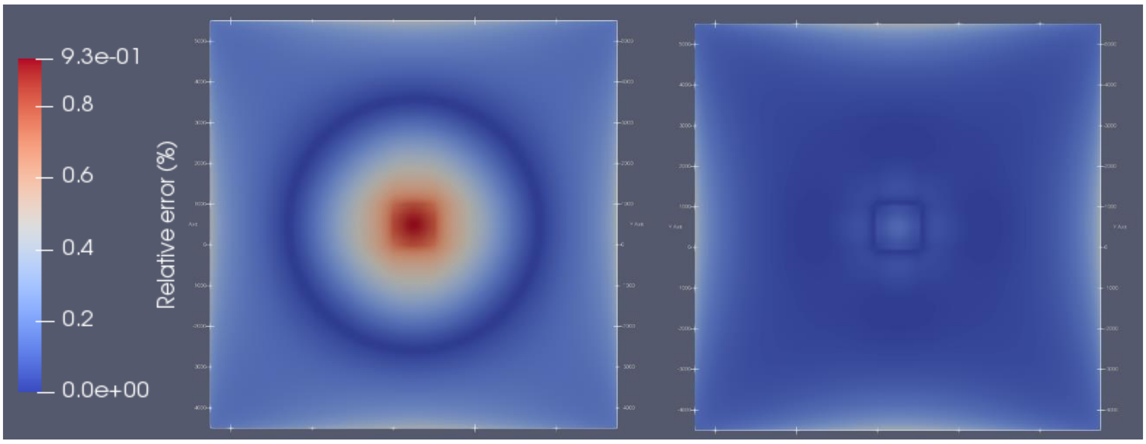

Fig. 4.7: Top view of the calculated absolute norm relative error on the extended grid to the right, and the non-extended grid to the left (ParaView visualization).

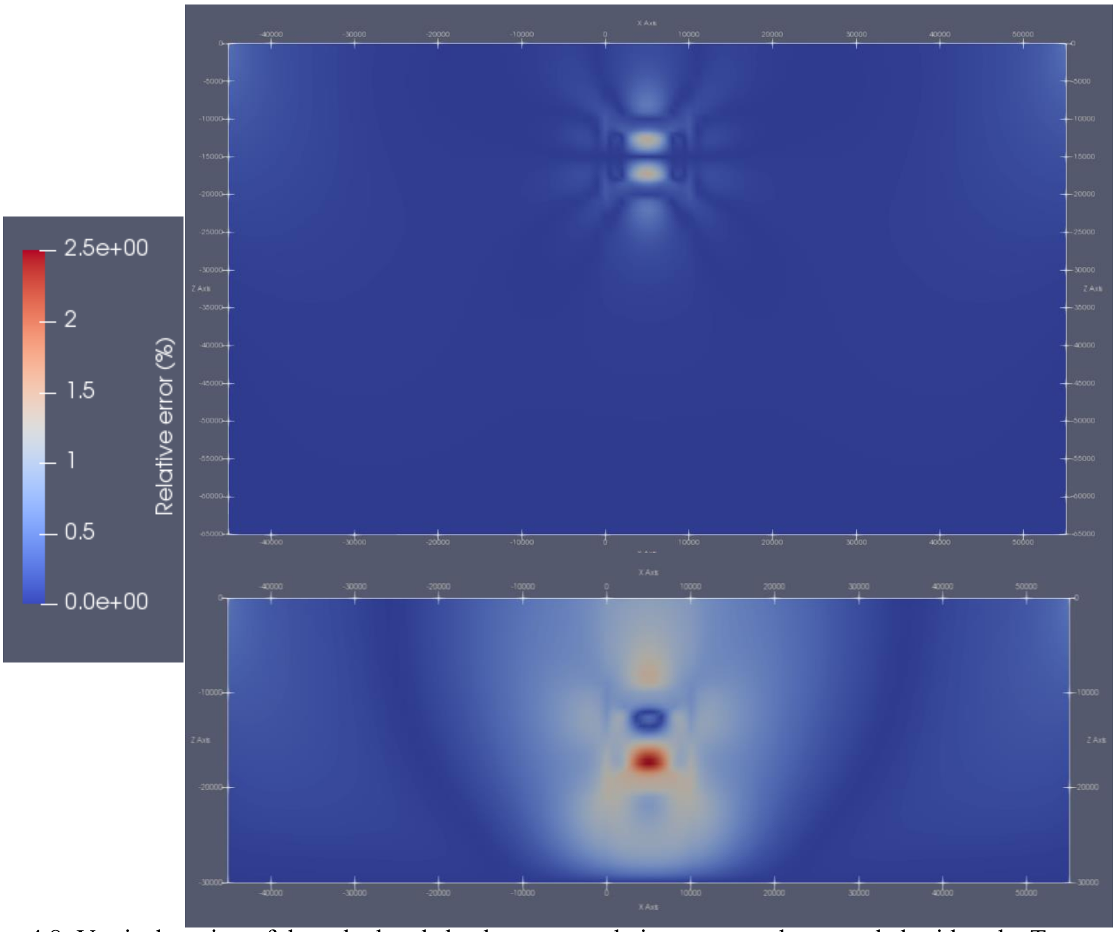

Fig. 4.8: Vertical section of the calculated absolute norm relative error on the extended grid to the Top, and the non-extended grid to the Bottom (ParaView visualization).

Tab. 4.3: Summary of Calculated discrepancies of VEM solution with respect to the FEM solution.

	Non- Extended grid	**Extended grid**
Maximum solution discrepancy at the surface (subsidence) in (%)	0.92	0.42
Maximum solution discrepancy over the whole volume in (%)	2.54	1.37

In Figs 4.7 and 4.8, we show the effects of the boundary conditions applied on the bottom plane perpendicular to the z coordinate axis on the solution discrepancy between the two grid-extension scenarios. For the non-extended grid, we report that once the solution reaches the boundary, it reflects back, inducing larger discrepancies over the whole displacement field and more precisely at the pressure depletion source with respect to the whole volume, and at the center of the subsidence bowl with respect to the surface level. The comparison performed over the extended grid is deemed satisfactory given that the maximum discrepancy is lower than 1%.

Coherently, the possible sources for solution discrepancy over the extended grid are:

- The pressure extrapolation methodology.
- The intrinsic numerical approximations of the FEM/VEM in solving the stress-strain problem.

While, the boundary conditions may increase this discrepancy up to 2.54%, the VEM approximation remains acceptable with regards to the considered vertical grid extension.

The discrepancy is lower at the surface level because of the formulation we used to estimate the absolute norm relative error, where higher displacements are adjacent to the source generating the pressure drop, rendering the difference between the nodal solutions at that level generally one order of magnitude higher than the ones calculated at the surface.

To conclude, the numerical solution provided by the Virtual element method is deemed representative and accurate with respect to the FEM solution, given that the discretization used is **a regular structured grid** with no deformations for both the geomechanical volume and the pressure source volume.

4.2. Realistic model:

4.2.1. Geological context:

Petroleum systems occurrences (Gas/oil fields) in Italy are the result of complex geological processes (plural tectono-stratigraphic cycles) that have taken place within the Italian peninsula and the Adriatic Sea Fig. 4.10 [39] [40].

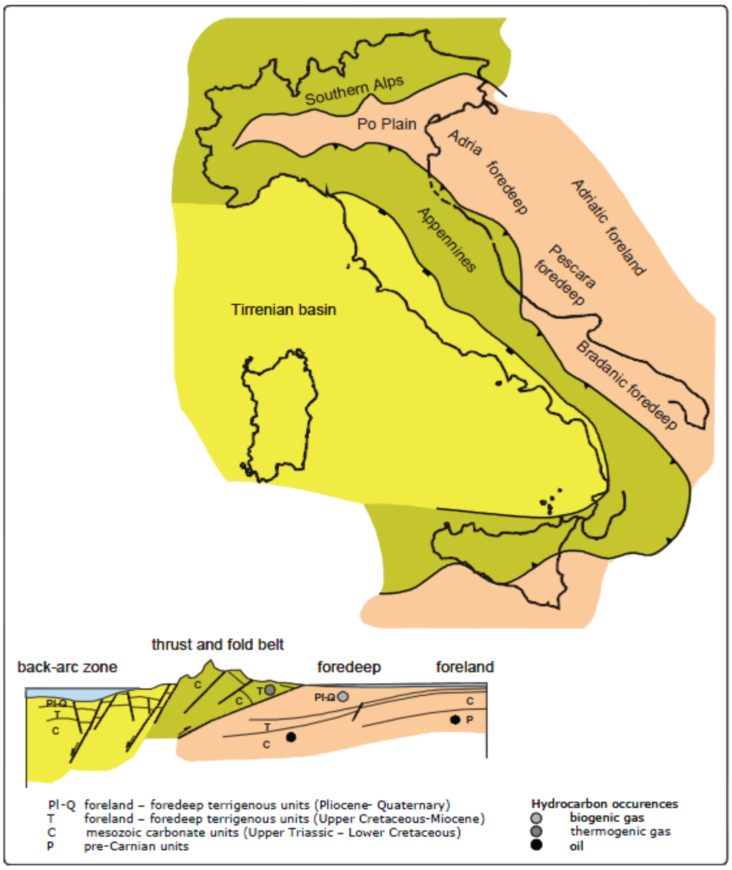

Fig. 4.9: Oil and gas occurrences within the Italian peninsula.

The considered source rocks were formed due to the Apennine thrusting from the Miocene to late Pliocene. During which, suitable conditions favored the biogenic gas generation: [41]

- High sedimentation rate.
- Low geothermal gradient.

The bearing reservoir rocks can be structural traps, where the biogenic gas accumulated in anticlines situated in the internal part of the foredeep adjacent to the Apennines thrust belt. These traps were formed during the late Pliocene and early Pleistocene as a result of the Apennine compression. Prompting a significant vertical displacement from 800-1000 m, ideal for the super-positioning of gas pools. As for the external part, gentle anticlines formed due to differential compaction of turbidites sandstones over the same geological era, yet they are considered stratigraphic traps as they are sealed up-dip (pinchout) by shales (argille del Santerno) Fig. 4.11 [39][40].

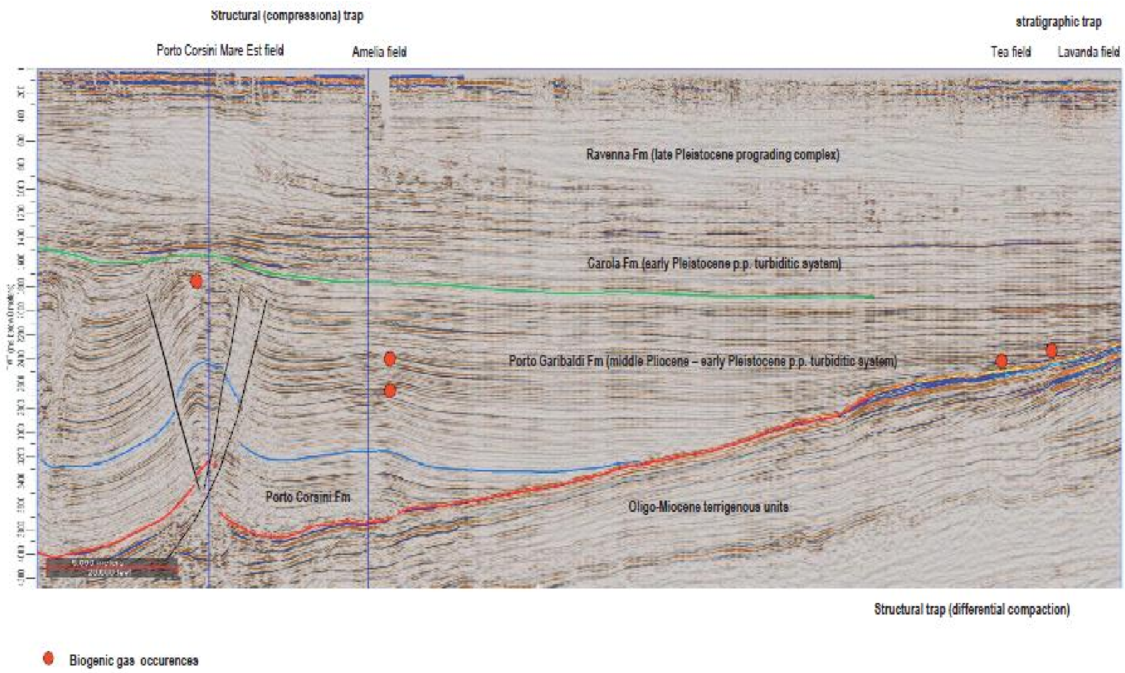

Fig. 4.10: Seismic profile highlighting the stratigraphic and structural traps of biogenic gas [40].

The gas reservoirs are found within the Po Plains which expand over the Northern Adriatic and majority of Central Adriatic. They are the result of depositional successions mainly from turbidities mainly from environments. These successions consist of sequential cycles of turbidite cycles alternating between sandy deposits and shaly deposits leading to interbedded sandstone bearing rocks and shales forming mainly multilayered reservoirs. [39][40][41]

4.2.2. Case study:

The available geological data provided the possibility to build a 3D representative model of the lithology of an offshore field within the Northern part of the Adriatic Sea. With the help of the literature and seismic data gathered over the whole region [39] [40] [41] [42], integrated with well-logs interpretation, it was possible to represent the real lithology Fig. 4.11 in an adequate manner.

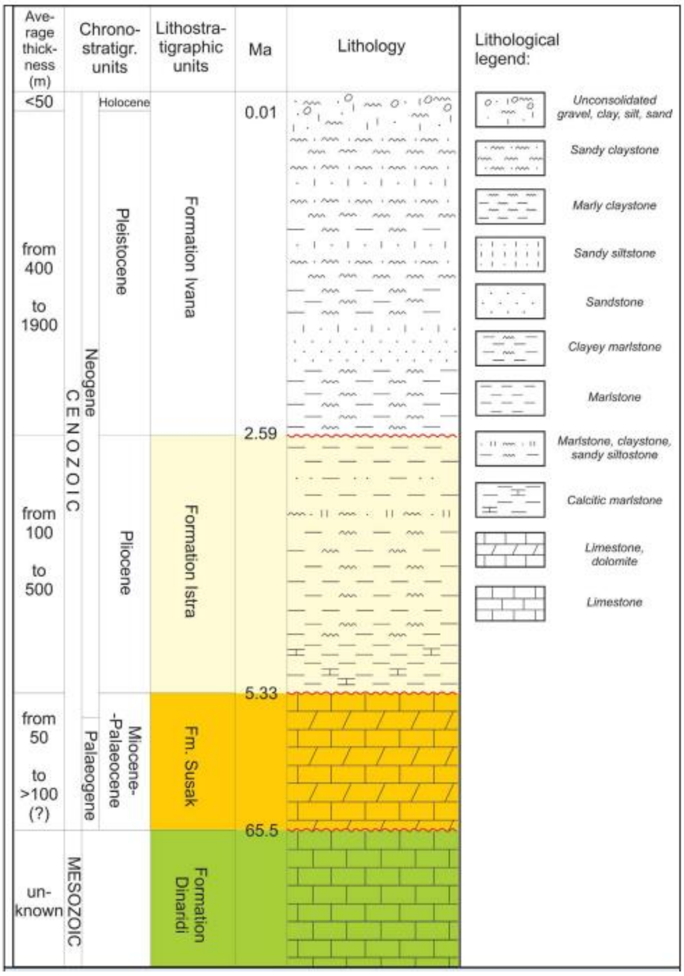

Fig. 4.11: Lithostratigraphy and lithofacies in Northren of Adriatic (croatian waters) [42].

In particular, each strata was represented as a grid portion storing mechanical properties specific to each formation as shown in Tab. 4.4. The synthetic model also reproduces a thinning of the Carola formation forming a pinch-out as shown in the Fig.4.12.

Tab. 4.4: Stratigraphic zones of the 3D model.

Age	Formation	lithology	Zone reference in the model	horizon depth (m TVDs)	Surface
Holocene	Ravenna	Marine sands	0	-37	Top 1 Ravenna
Pleistocene		Clays with local sand interlayer	1	-70	Top 2 Ravenna
			2	-270	Top Carola
	Carola	Alternating thin sands and clays	3	-712	Top Reservoir
			4	-742	Bottom Reservoir
			5	-842	Top Santerno
Pliocene	Saterno	Clays	6	~	Top Basamento
Cenosoic-Mesozioc	Basamento	Marls and calcareous marls	7	~	

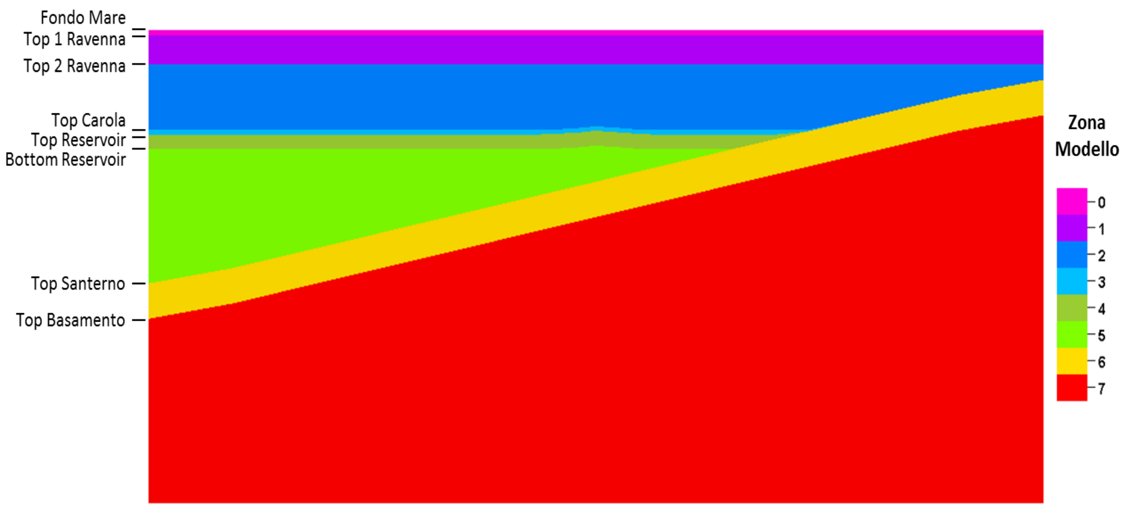

Fig. 4.12: Scheme representative of the stratigraphic zones.

The synthetic reservoir model is represented by an anticlinal gas bearing formation Fig.4.13. It is a gas pool within the Carola formation Fig. 4.14, while the Ravenna formation provides the impermeable clay seal to trap the gas. The reservoir is characterized by a homogeneous distribution of the petrophysical properties over the whole domain. The productive zone is not supported by any aquifer. Therefore, the volumetric depletion (gas expansion) becomes the main production drive mechanism.

Tab. 4.5: Reservoir data.

Reservoir	**Datum level (m TVDs)**	**pressure @Datum (barsa)**	**Porosity (-)**	**NTG (-)**	**Irreducible water saturation (-)**
Silty sandy Gas bearing formation.	-714	79	0.3	1	0.266

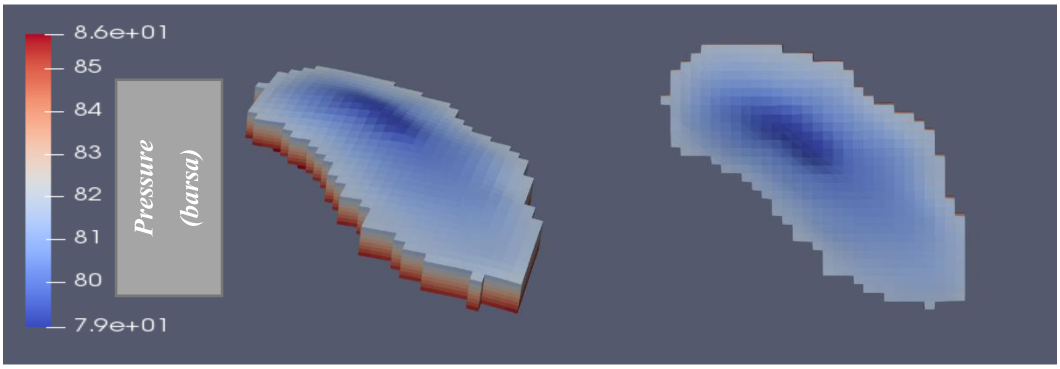

Fig. 4.13: Initial pressure distribution of the reservoir's (ParaView visualization).

The Geomechanical Volume was populated based on the collected mechanical data [42][39] [40][41][42], and the routine laboratory triaxial tests CID and CIU performed on rock samples taken from gas wells producing within the same region, Fig. 4.14 and Tab 4.6. The volume is assumed to be homogeneous, isotropic and linear elastic.

Fig. 4.14: geomechanical classes.

Tab. 4.6: Geomechanical Parameters distribution.

<table>
<tr><th>Geomechanical Class</th><th>Young's Modulus (GPa)</th><th>Poisson's ratio (-)</th><th>Bulk Density (g/cm^3)</th><th>Biot Coefficient</th></tr>
<tr><td>1</td><td>0.03</td><td rowspan="2">0.38</td><td>1.8</td><td rowspan="6">1</td></tr>
<tr><td>2</td><td>0.4</td><td>1.9</td></tr>
<tr><td>3</td><td rowspan="3">0.0046z+0.3082</td><td rowspan="3">0.35</td><td>2.1</td></tr>
<tr><td>4</td><td>2.2</td></tr>
<tr><td>5</td><td>2.3</td></tr>
<tr><td>6</td><td>65</td><td>0.3</td><td>2.6</td></tr>
</table>

A production scenario was planned to impose a 40 bars pressure drop over a 4 years period, from March, 23rd 2018 to March, 23rd 2022.

In order to analyze the depletion induced subsidence, we considered these Hypotheses as a starting point for our simulations:

- The geomechanical model response to production isotropic and linear elastic.
- The petrophysical parameters (permeability and porosity) are assumed to remain constant over the production period and are not affected by the stress-strain variations caused by the reservoir's compaction.
- The contrast of elastic moduli between the reservoir and its surroundings is negligible, reducing the arching effects.

4.2.3. Technical considerations for geomechanical model building and data processing :

4.2.3.1. Coupling technique selection:

Ideally, adopting a fully coupling technique provides a complete and an accurate solution, since the fluid flow and geomechanical problem are solved simultaneously taking into account the reciprocal dependencies of the involved parameters. However, we opted for a modular approach i.e. solving the strain-strain set of equations independently from the multiphase flow simulation. In the technical literature such approach is called the De-coupled approach (or the one way coupling approach). We have chosen this alternative for several reasons related to technical limitations, benchmarking requirement and literature references.

It is technically challenging at this stage of the work to adopt a higher coupling degree. In this phase of the study, we compare the approximated displacements by two numerical methods, induced by the same production history. For this purpose, any parameter (i.e. permeability and porosity) that can influence the reservoir's pressure evolution during the geomechanical simulation is kept constant. Higher degrees of coupling may lead to different pressure redistribution profiles between the two simulators, generating different pressure values at the centroids and consequently at nodes. While considering the different extrapolation techniques used by the simulators, adding a new level of complexity by the adoption of a higher coupling strategy, there is a possibility that the FEM and VEM methods will not simulation the same pressure-scenario. Therefore, for a more fair results comparison, the one-way approach is most suitable, because it offers the best possibility of control over the parameters that can cause pressure input-discrepancies.

In addition, we refer to results shown in - [21] (Numerical Techniques Used for Predicting Subsidence Due to Gas Extraction in the North Adriatic Sea), and - [22] (A Coupled Fluid Flow - Geomechanical Approach for Subsidence Numerical Simulation). In these two papers, the effects of different coupling approaches are analyzed on the history matched model of Dosso Degli Angeli field - [21], and on a synthetic mode constructed referring to lab/literature data gathered with reference to the Adriatic basin - [22], similarly to the case study our synthetic model is built on. Both studies deduced that the one way approach provides accurate results for subsidence in gas fields, while the two-way approach is deemed more representative in the presence of an aquifer or at reservoir level (compaction).

4.2.3.2. Pinchout related issues:

The geometrical modeling of a gradual stratigraphic thinning of beds (pinch-out), is translated in structured meshes by a decrease of cell's thickness until they become null. Such configuration leads to nodes collapsing as Fig. 4.15 shows. Subsequently, the resulting grid exhibits node connections that are not related physically. They are called Non-Neighboring connections.

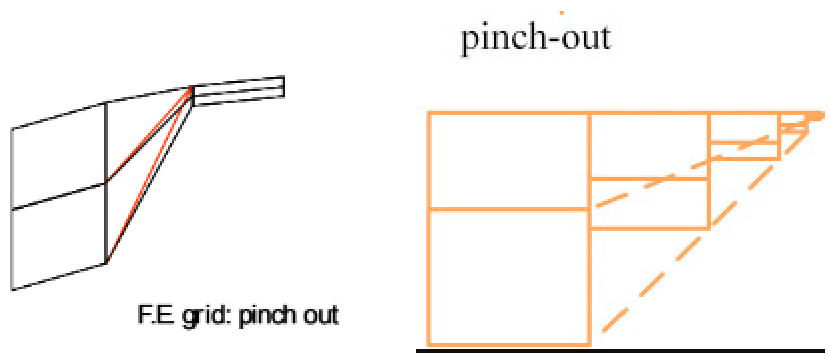

Fig. 4.15: Pinchout scheme in the FE domain

Petrel automatically identifies these new connections created upon surface/horizon implementations and classifies the cells with zero thickness as inactive cells so they would be neglected during the solution process. Yet, they are still present in the grid. Therefore, to handle correctly the grid conversion, it is necessary to identify the non-neighboring connections.

However, the topology exported via batch process doesn't eliminate collapsed cells from the exported topology as opposed to Petrel geomechanics output that contain only active cells. The resulting grid differs in term of number of cell and the related numbering. Hence, a series of commands were added to the concerned Matlab script that converts the file to a VTK extension. These commands cross-reference the Petrel's output with the Visage one and flags out any non-neighboring connections in order to obtain an improved VISAGE .VTK file ready for the comparison.

4.2.4. Volume Discretization Scenarios:

This thesis work deals with the assessment of solutions approximated by the Virtual Element method when simulating the subsidence phenomena over four different volume discretizations. The results are then compared against the FEM simulation provided by the Petrel commercial software.

The geomechanical volume dimensions are kept constant over the different scenarios, x×y×z (35913.7m×35200m×3200m). At this stage of our work, the boundary conditions are made sure to not interfere with the solutions.

Unstructured grid: tetrahedral Mesh

As a starting point, we comply with the VEM hypothesis, by testing it over an unstructured mesh Figs.4.16 and 4.17, identified by tetrahedral cells over the whole geomechanical volume, including the reservoir's grid.

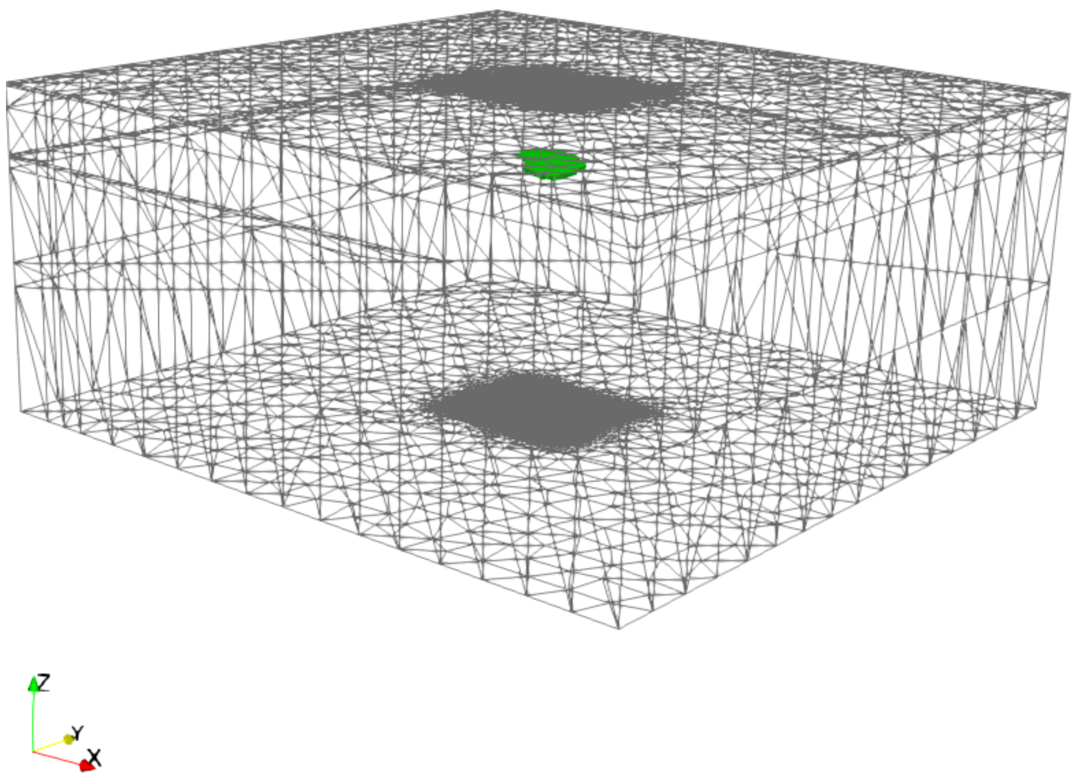

Fig. 4.16: The 3D geometrical representation of the geomechanical volume over an unstructured mesh (ParaView Visualization).

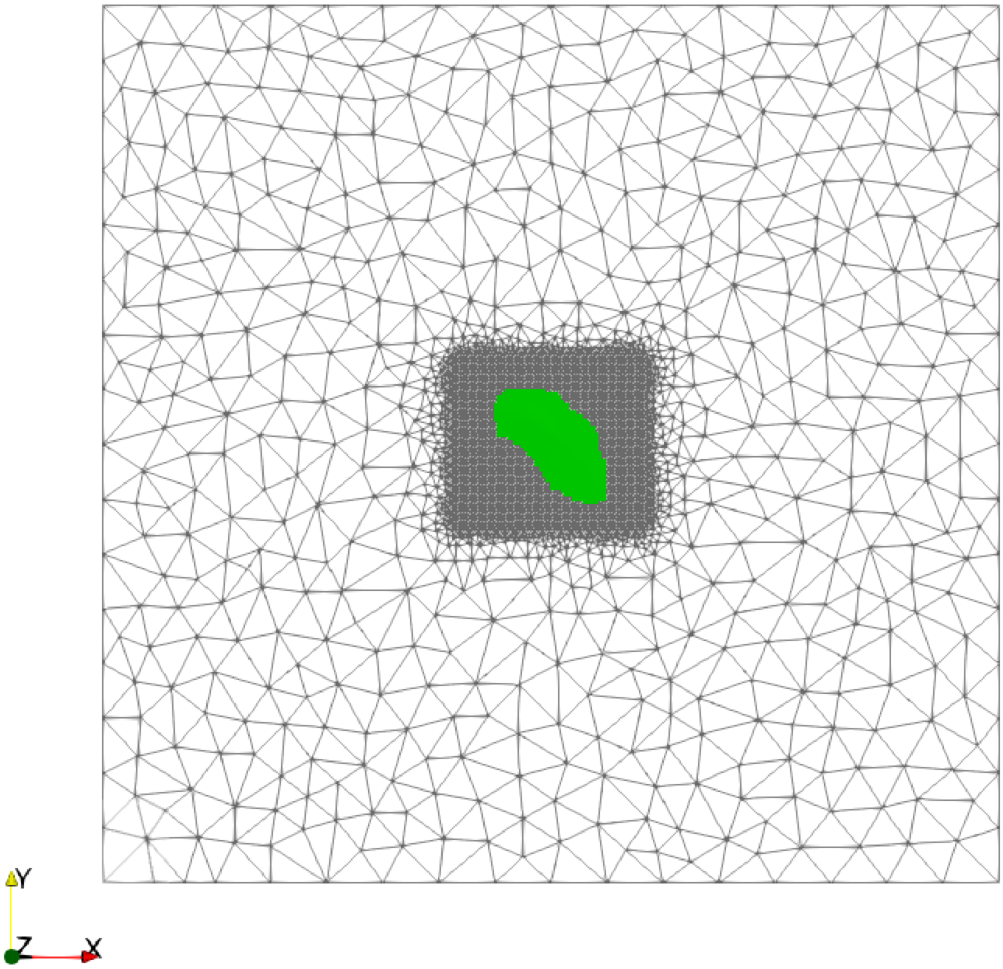

Fig. 4.17: Top view of the 3D geometrical representation of the geomechanical volume over an unstructured mesh (ParaView Visualization).

Tab 4.7: Information about mesh discretization.

	STRUCTURED MESH		UNSTRUCTURED TETRAHEDRAL MESH	
	Reservoir grid	**Full geomechanical volume**	**Reservoir grid**	**Full geomechanical volume**
NUMBER OF CELLS	5149	276700	34001	1104293
NUMBER OF NODES	6406	287818	6826	187494

Results :

The performance of VEM simulations in terms of vertical displacements over the tetrahedral mesh are shown Figs. 4.18 and 4.19 and Tab. 4.8. The results are compared against the FEM solution provided by Petrel Geomechanics.

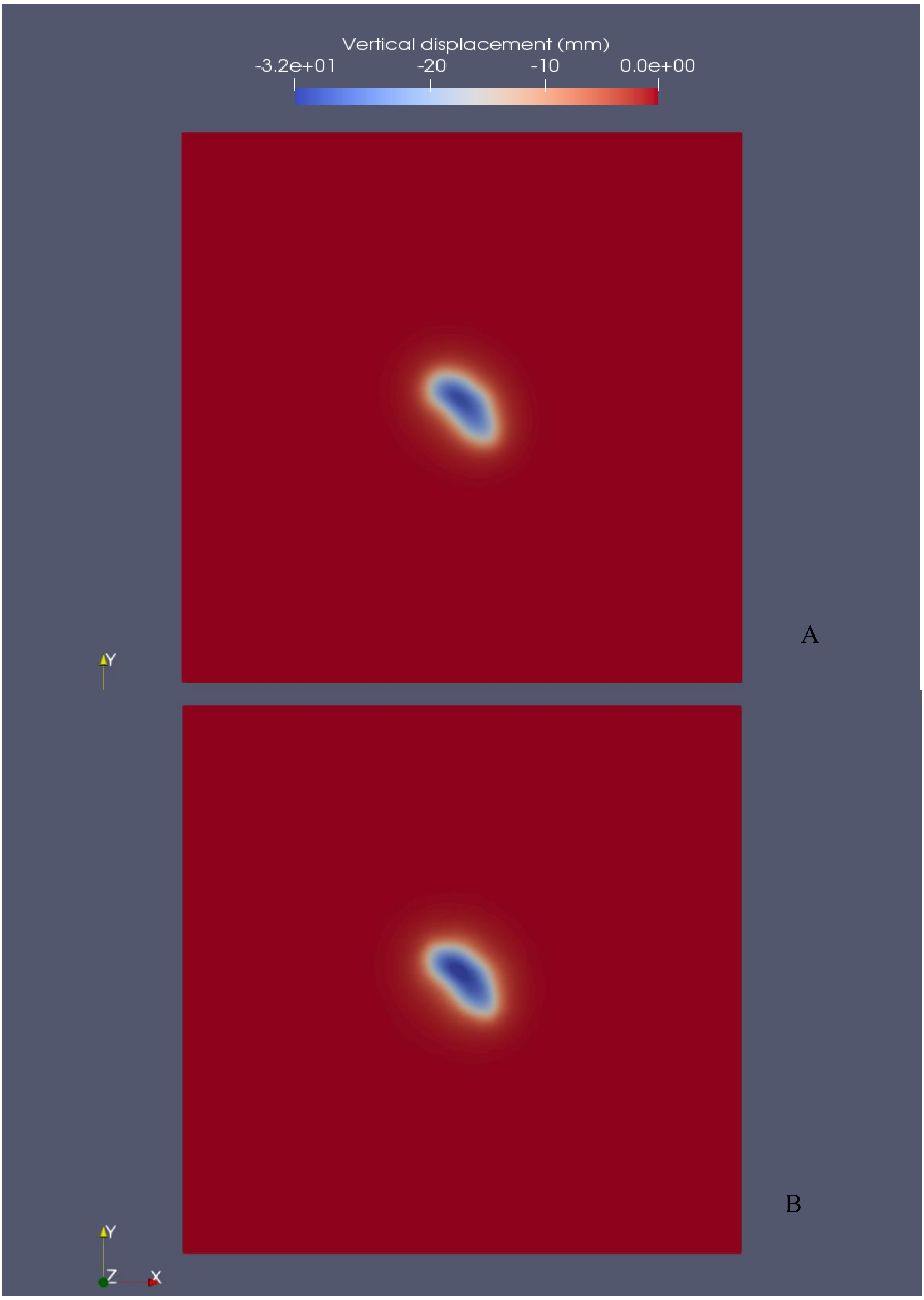

Fig. 4.18: Top View displaying the approximated subsidence over the whole geomechanical volume: A) FEM solution and B) VEM solution over the tetrahedral unstructured mesh (ParaView Visualization).

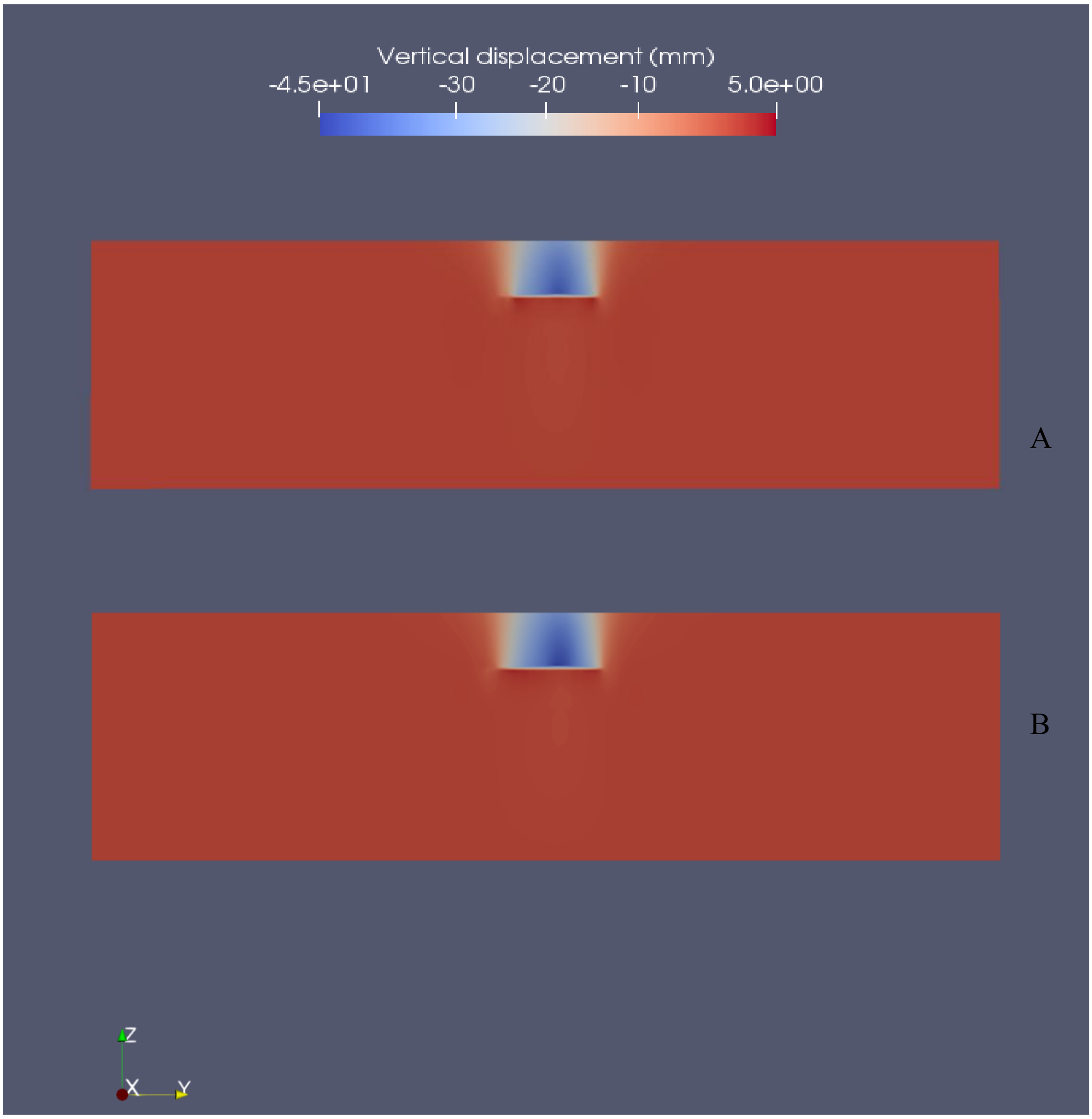

Fig. 4.19: Vertical section approximated displacements (along the z-axis) over the whole geomechanical volume: A) FEM solution and B) VEM solution over the tetrahedral unstructured mesh (ParaView Visualization).

Tab. 4.8: Summary of Calculated displacements of VEM solution over the tetrahedral unstructured mesh.

	FEM solution	**VEM solution over the unstructured mesh**
Maximum displacement at the surface (subsidence) in mm	-30.8897	-33.1450
Maximum displacement over the whole volume in mm	-42.7726	-45.4396

The numerical solution of VEM over the tetrahedral discretization scenario provides comparable results with the FEM solution. We report that it overestimates the subsidence by a difference of few millimeters, but the phenomenon is properly represented.

Structured grid: Regular hexahedral grid

The second discretezation tested on VEM is the regular structured grid (corner point) Figs 4.20 and 4.21. The discrtezied mesh is identified by hexahedron cells. We test the VEM method directly on the original grid generated by Petrel, on which the FEM solution is computed.

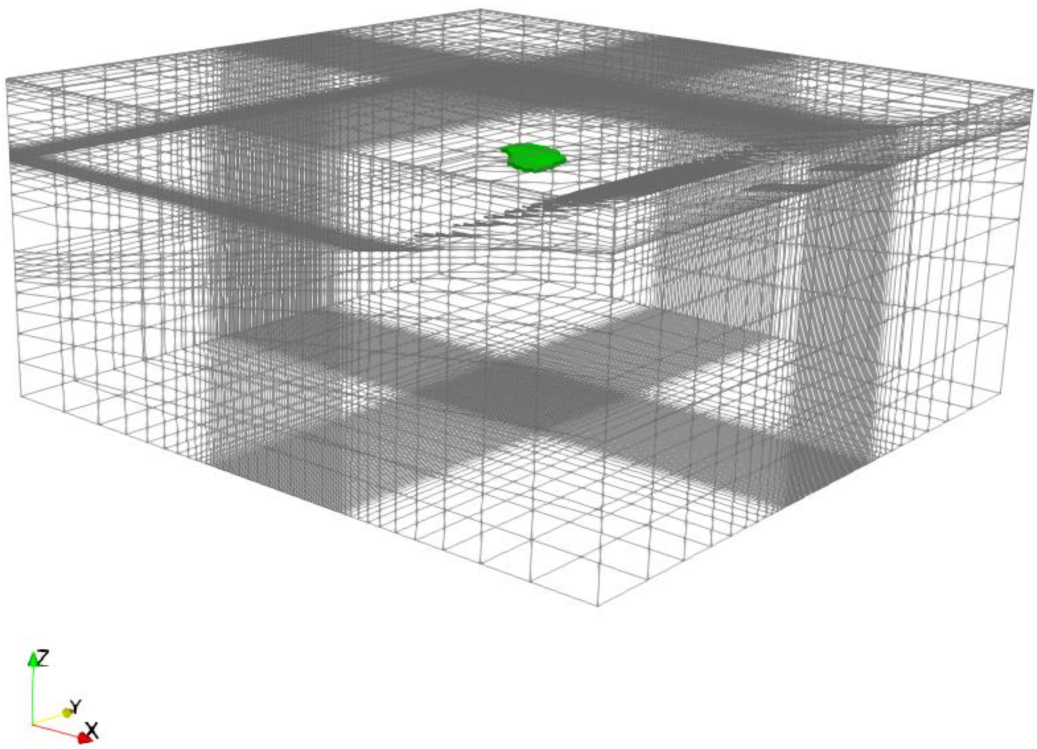

Fig. 4.20: The 3D geometrical representation of the geomechanical volume over a regular structured hexahedron grid (ParaView Visualization).

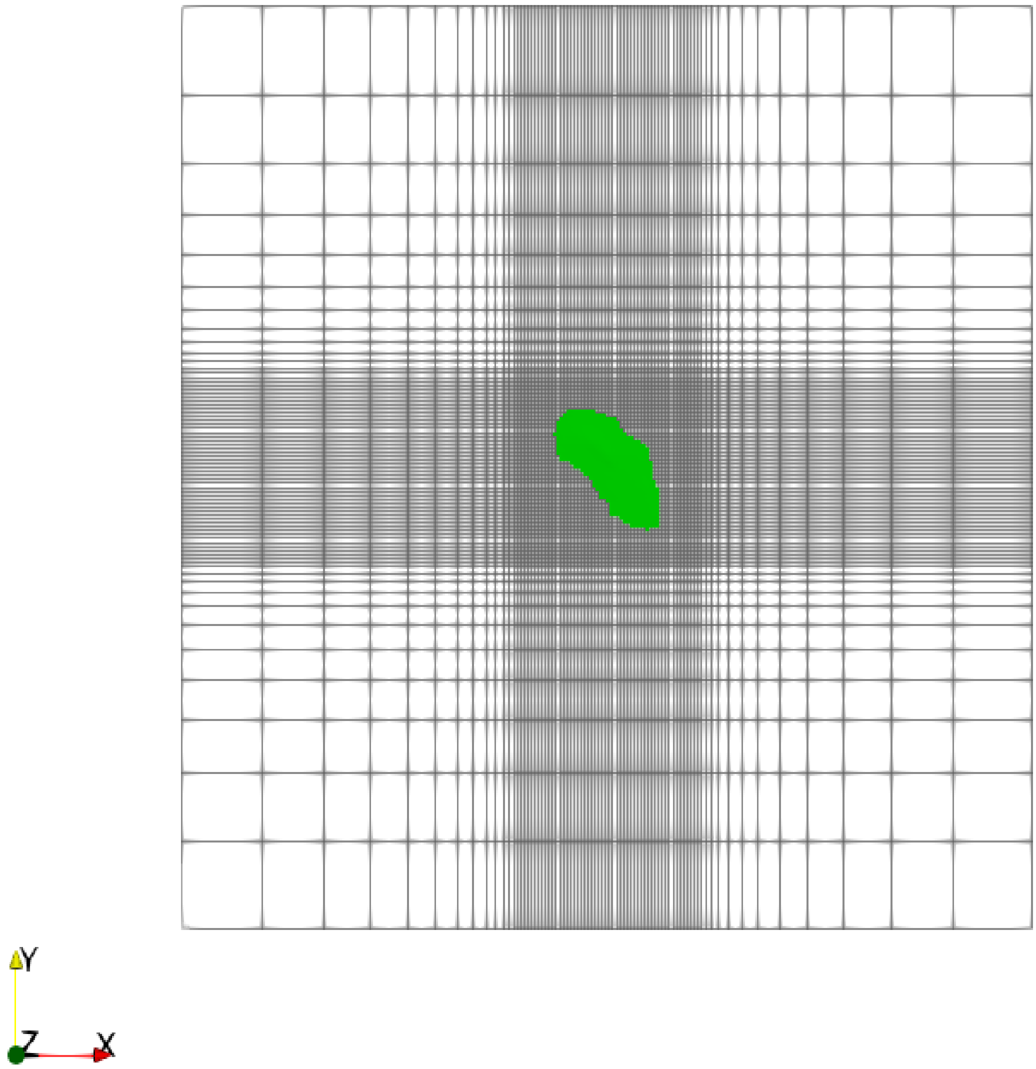

Fig. 4.21: Top view of the 3D geometrical representation of the geomechanical volume over a regular structured hexahedron grid (ParaView Visualization).

Results:

The performance of VEM simulations in terms of vertical displacements over the structured mesh are shown Figs. 4.22 and 4.23 and Tab. 4.9. The results are compared against the FEM solution provided by Petrel Geomechanics.

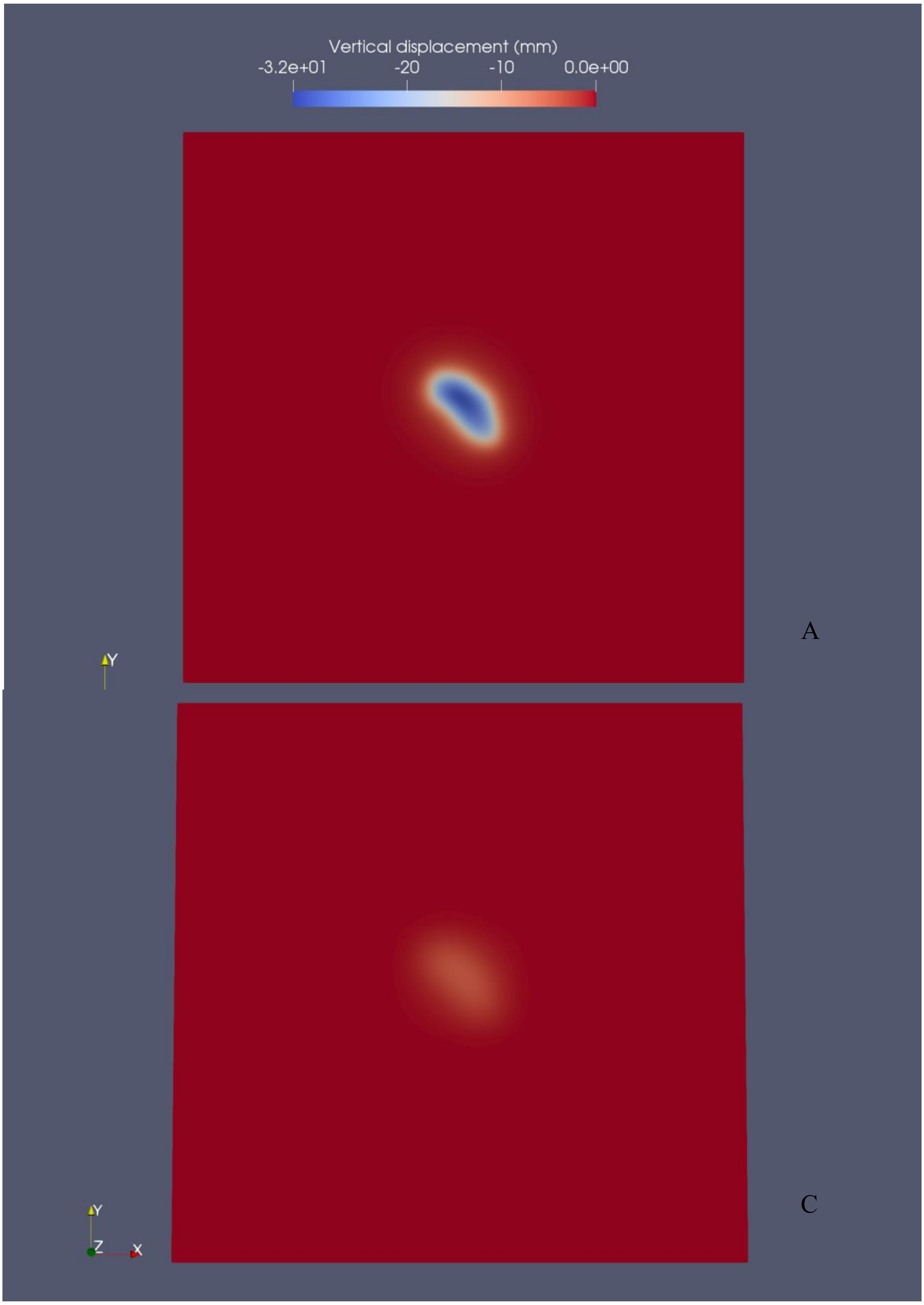

Fig. 4.22: Top View displaying the approximated subsidence over the whole geomechanical volume: A) FEM solution and C) VEM solution over the regular structured mesh (ParaView Visualization).

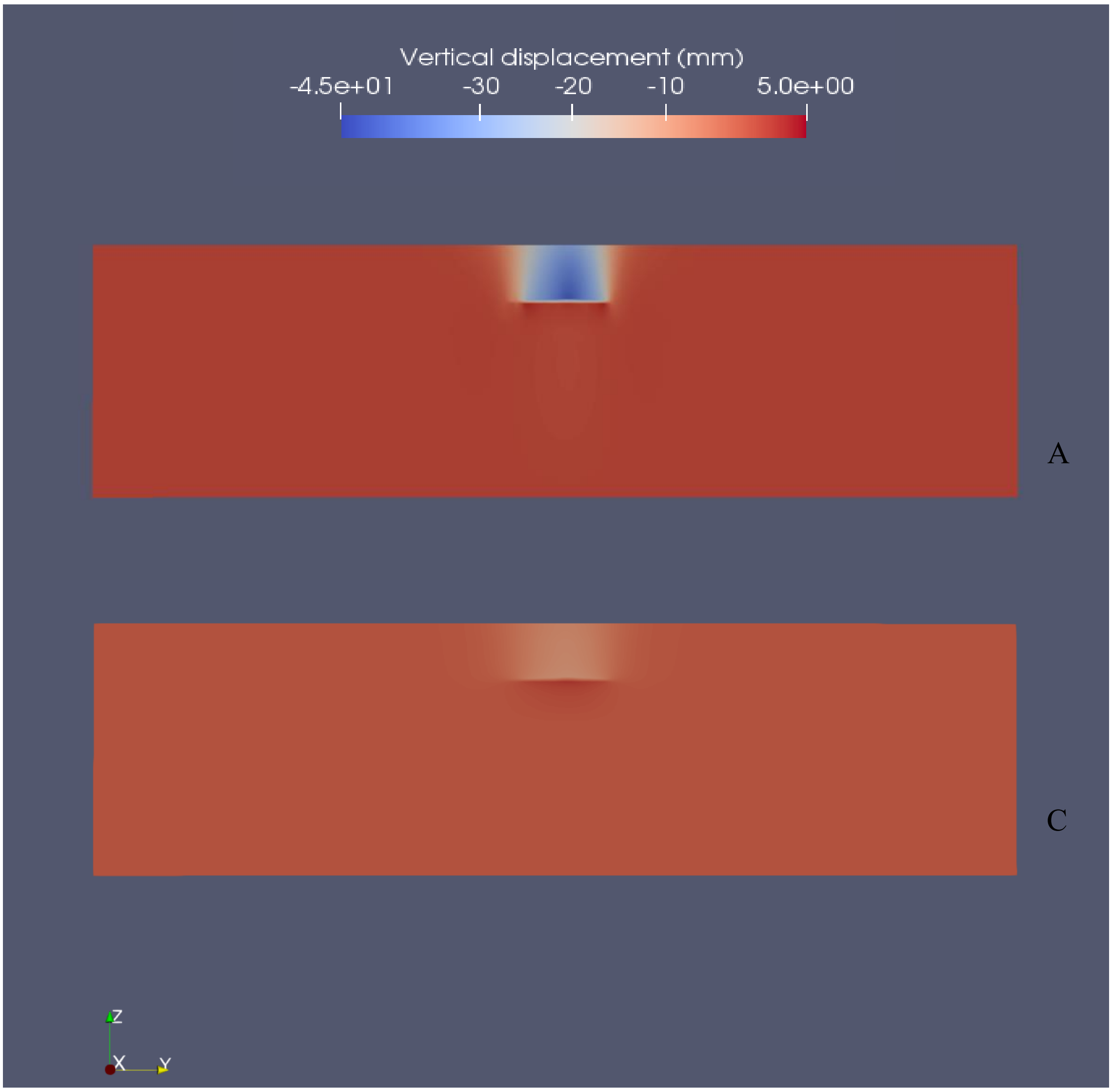

Fig. 4.23: Vertical section approximated displacements (along the z-axis) over the whole geomechanical volume: A) FEM solution and B) VEM solution over the regular structured mesh (ParaView Visualization).

Tab. 4.9: Summary of Calculated displacements of VEM solution over the regular structured mesh.

	FEM solution	**VEM solution over the regular structured mesh**
Maximum displacement at the surface (subsidence) in mm	-30.8897	-4.4969
Maximum displacement over the whole volume in mm	-42.7726	-5.9624

From the results obtained, the VEM solution failed to reproduce the subsidence phenomena properly, as it underestimates greatly the displacements at the reservoir level (with a difference > 35 mm). In addition, it did not properly reproduce the displacement field in the above overburden zone up to the surface, as the highest displacements are concentrated directly above the reservoir. The remaining overburden seem to fairly witness variations within the range of 1 millimeter as opposed to the FEM solution up to 11 millimeters. This suggests that the accuracy of the computation deteriorates at the reservoir level.

To explain the failed VEM response we refer to – [10] (Basic principles of Virtual Element Methods. Mathematical Models and Methods in Applied Sciences) and - [49] (Virtual element method for geomechanical simulations of reservoir models). The paper suggests that the method doesn't handle complex geometries for deformed cells. This means that the reservoir's anticlinal topology can be the source of the solution discrepancy.

When constructing the strucutred mesh to represent the reservoir, the resulting hexahedron cells have non perfectly planar faces[14] Fig. 4.24, to properly recreate the curvature of the anticline.

It is observed that the tetrahedral unstructured grid have proven comparable with the FEM solution, because triangular faces implcitily satisfy the planarity requirement.

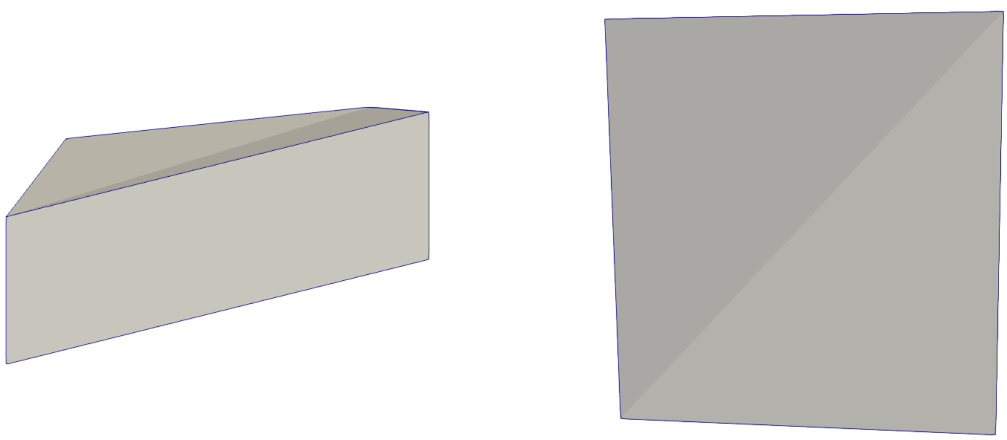

Fig. 4.24: 3D representation of isolated hexahedron cells from the top of the reservoir with cruved faces (ParaView Visualization).

[14] A planar face is established when all its vertices define one plane.

Structured grid: hexahedral meshing with general polyhedral discretization at the reservoir formation level:

We take as a reference, the work done in - [34] (Virtual element method for geomechanical simulations of reservoir models) providing a primary mitigative solution to the issue of non-planar cells. A Matlab script was used to recognize the faces that don't satisfy the planarity requirement, then it adds a barycenter to split the surfaces, into 4 planar triangle face. In Figs 4.25 and 4.26 we can see the original hexahedron cell with non-planar faces converted to a polyhedron cell with triangulated faces.

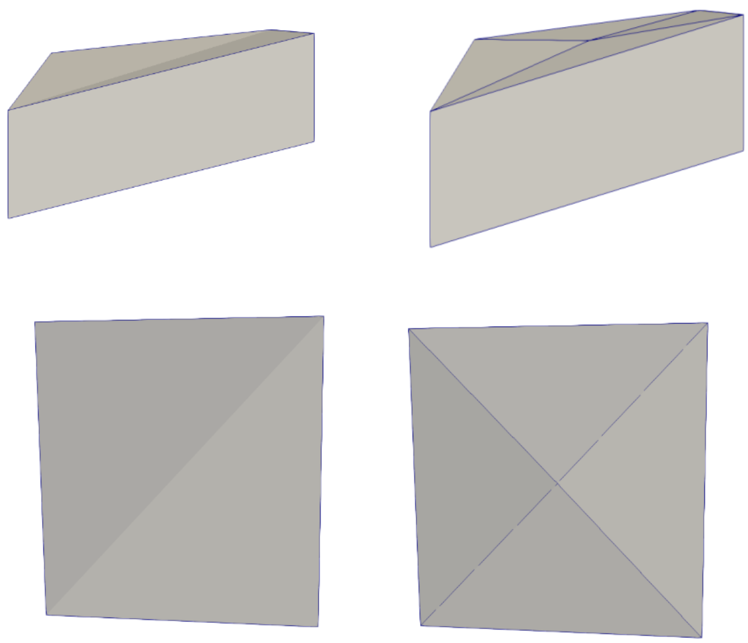

Fig. 4.25: 3D representation of hexahedron cells with curved faces to the left, and the same processed cell and converted into a general polyhedral with split triangulated faces to the right (ParaView Visualization).

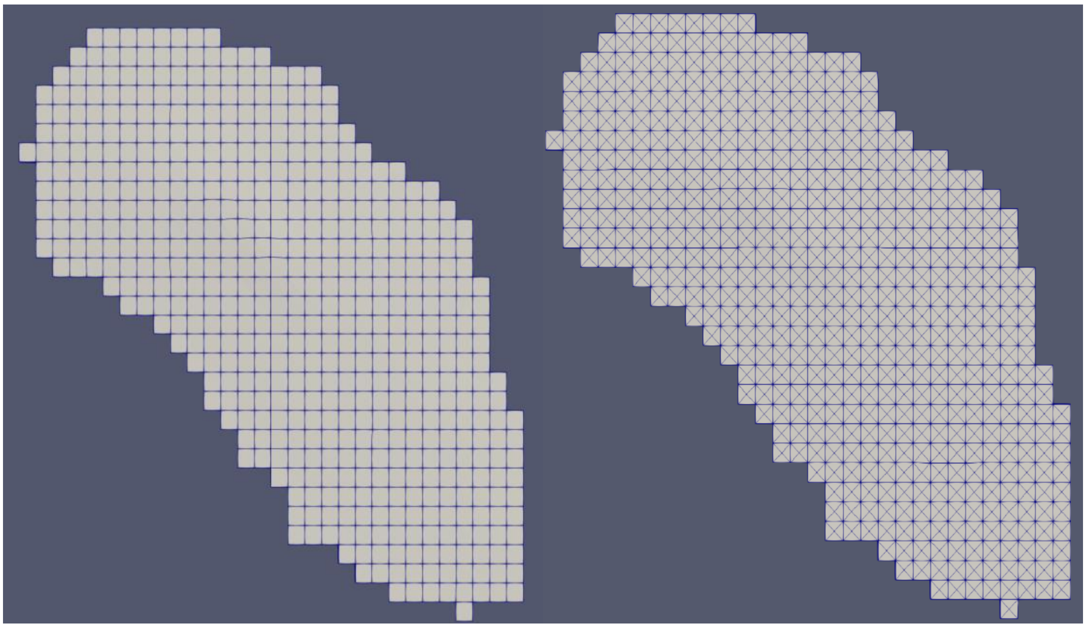

Fig. 4.26: Top view of 3D representation of the reservoir grid: Hexahedral cells to the left, and the processed polyhedral cells to the right (Paraview visualization).

A third grid is then constructed that contains a hybrid of polyhedra with triangulated faces within the reservoir level and the surrounding region while retaining regular shaped hexahedron cells over the remaining geomechanical volume. It'simportant to mention that while the number of nodes will increase, the number of cells remains the same with respect to the Petrel's grid Tab 4.10.

Tab 4.10: Information about mesh discretization.

	STRUCTURED MESH		STRUCTURED MESH WITH POLYHDERA WITH SPLIT FACES	
	Reservoir grid	**Full geomechanical volume**	**Reservoir grid**	**Full geomechanical volume**
NUMBER OF CELLS	5149	276700	5149	276700
NUMBER OF NODES	6406	287818	12092	355768

Results:

The performance of VEM simulations in terms of vertical displacements over the structured mesh are displayed in Figs. 4.27 and 4.28 and Tab. 4.11. The results are compared against the FEM solution provided by Petrel Geomechanics.

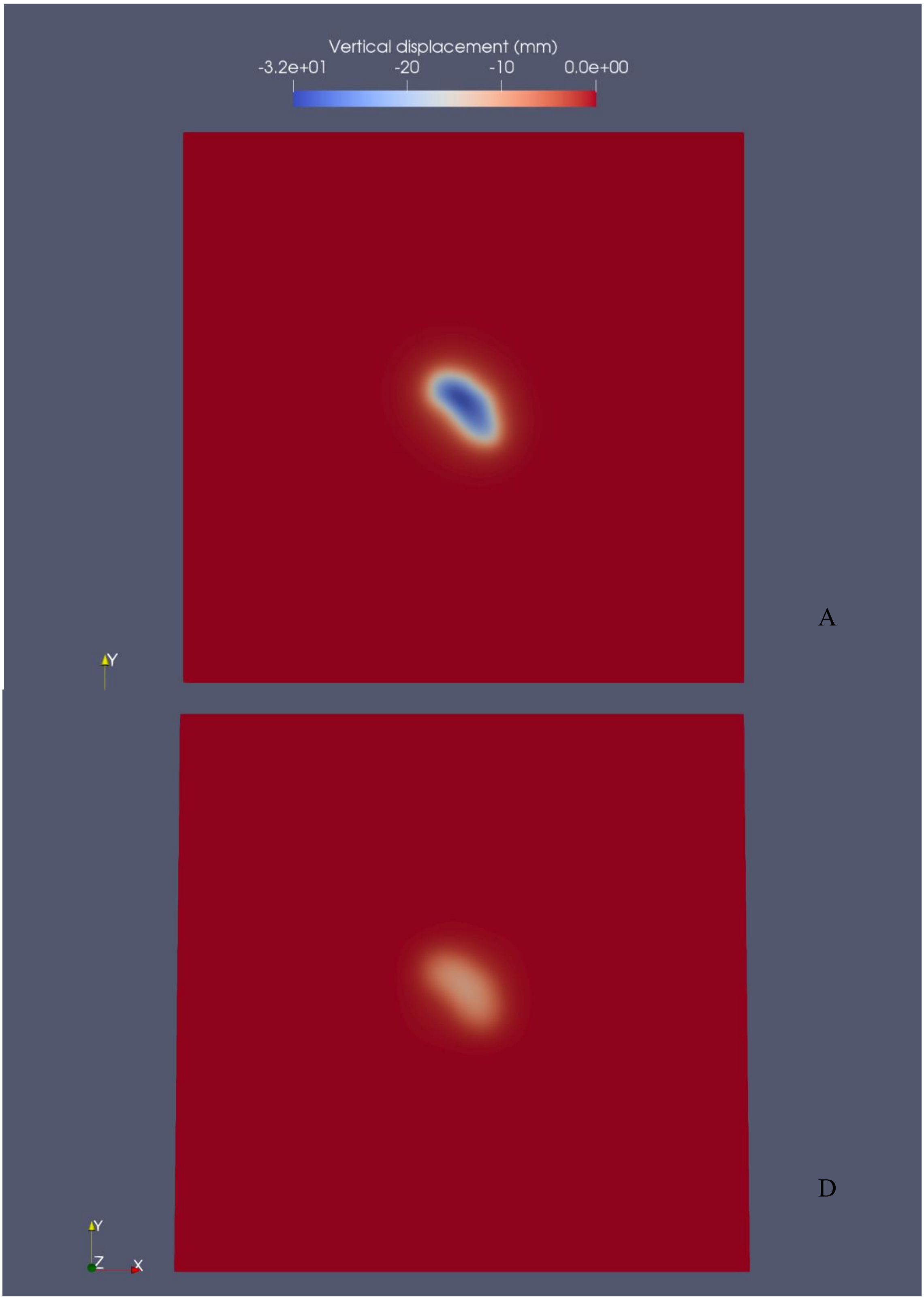

Fig. 4.27: Top View displaying the approximated subsidence over the whole geomechanical volume: A) FEM solution and D) VEM solution over the structured mesh with polyhdera identified by split faces (ParaView Visualization).

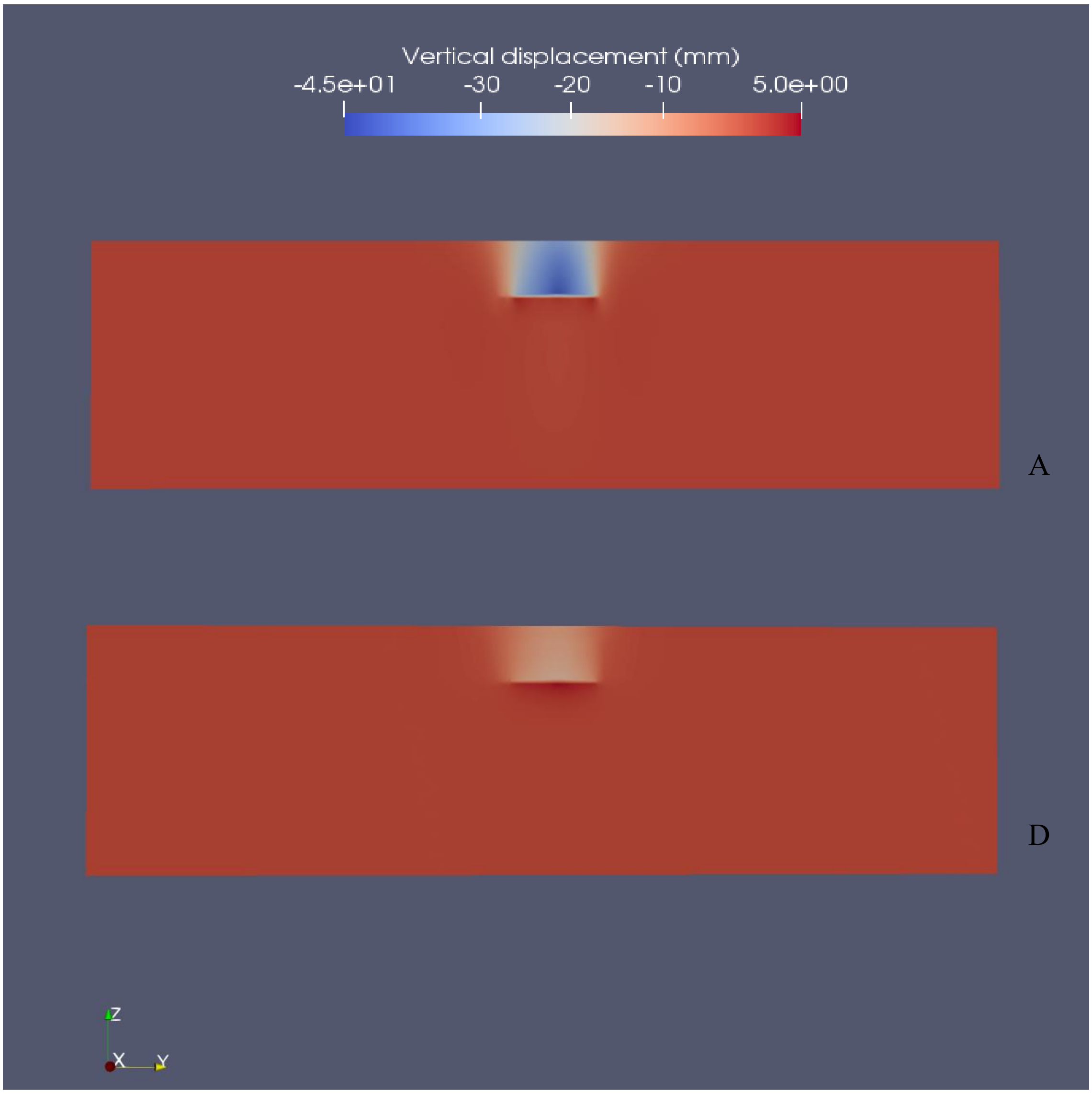

Fig. 4.28: Vertical section approximated displacements (along the z-axis) over the whole geomechanical volume: A) FEM solution and D) VEM solution over the structured mesh with polyhdera identified by split faces (ParaView Visualization).

Tab. 4.11: Summary of Calculated displacements of VEM solution over the structured mesh with general polyhedra.

	FEM solution	**VEM solution over the structured mesh**	**VEM solution over the structured mesh with general polyhdra**
Maximum displacement at the surface (subsidence) in mm	-30.8897	-4.4969	-10.7809
Maximum displacement over the whole volume in mm	-42.7726	-5.9624	-15.3301

By comparison with the previous case of the regular grid, the VEM solution, over a grid that satisfies the planarity requirement, shows a good improvement as the computed compaction went from 6 mm to 15mm. We also report that the displacements seem to be properly represented in both the reservoir and the surrounding zones. However, the results overall remain greatly underestimated within the reservoir level and consequently at the computed subsidence. This suggests that the degree of computation precision at the reservoir level is still too low. With reference to the Tabs 4.7 and 4.10, the unstructured mesh primarily used, contain a number of cells 66 times higher than the remaining two meshes, prompting the issue that the reservoir needs to be refined even further for an accurate numerical analysis. Therefore, the degree of accuracy of the solution provided by the VEM is possibly affected by the volume of the cells.

Hybrid grid: Structured geomechanical volume with tetrahedral meshing of the reservoir:

Building on the previous conclusions, we need to refine our grid even further at the reservoir level. A Matlab script was written, to split the polyhedral elements Fig. 4.29 into tetrahedral ones, in order to refine the reservoir's grid in addition to making sure the planarity requirement is respected. The resulting cells inplicitly satisfy both conditions.

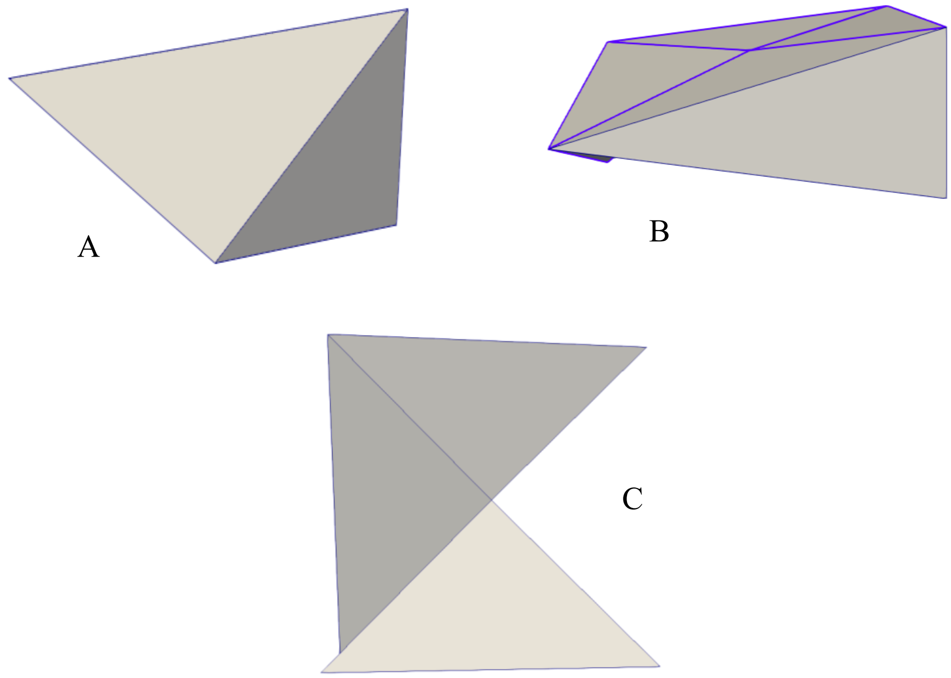

Fig. 4.29: Resulting tetrahedral cells after processing of polyhedral with split triangulated faces: A) regular tetrahedral cell, B) Vertical section of 4 connected tetrahedral cells, C) Top view of 3 connected tetrahedral cell, (ParaView Visualization).

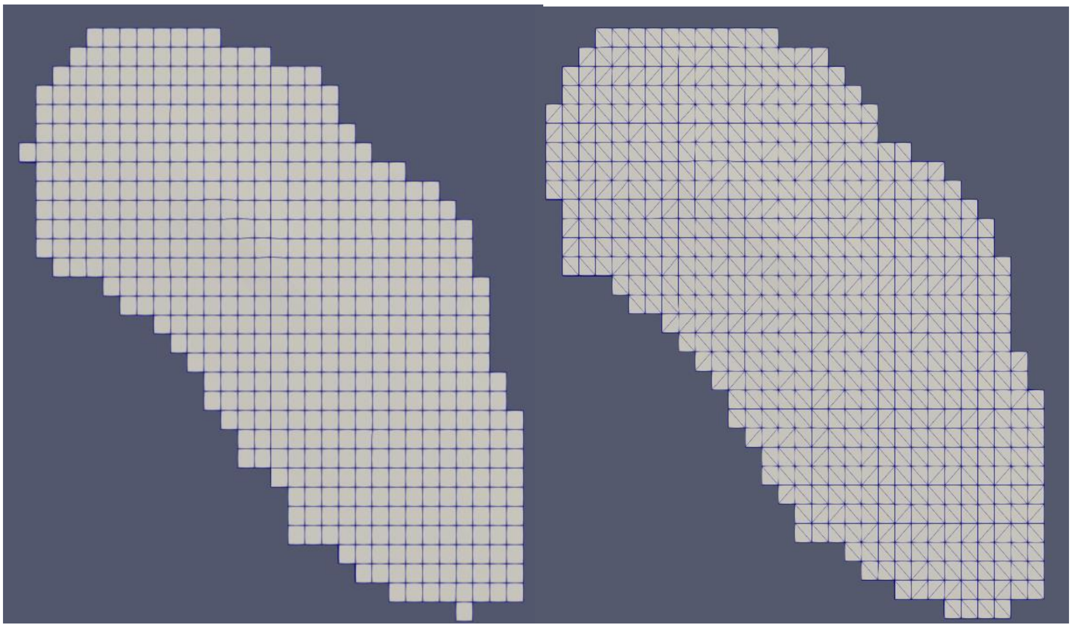

Fig. 4.30: Top view of 3D representation of the reservoir grid: Hexahedral cells to the left, and the processed polyhedral cells into tetrahedra to the right (Paraview visualization).

Tab 4.11: Information about mesh discretization.

	STRUCTURED MESH		HYBRID MESH	
	Reservoir grid	**Full geomechanical volume**	**Reservoir grid**	**Full geomechanical volume**
NUMBER OF CELLS	5149	276700	61788	333339
NUMBER OF NODES	6406	287818	12092	355768

Results:

The performance of VEM simulations in terms of vertical displacements over the structured mesh are displayed in Figs. 4.31 and 4.32 and Tab. 4.12. The results are compared against the FEM solution provided by Petrel Geomechanics.

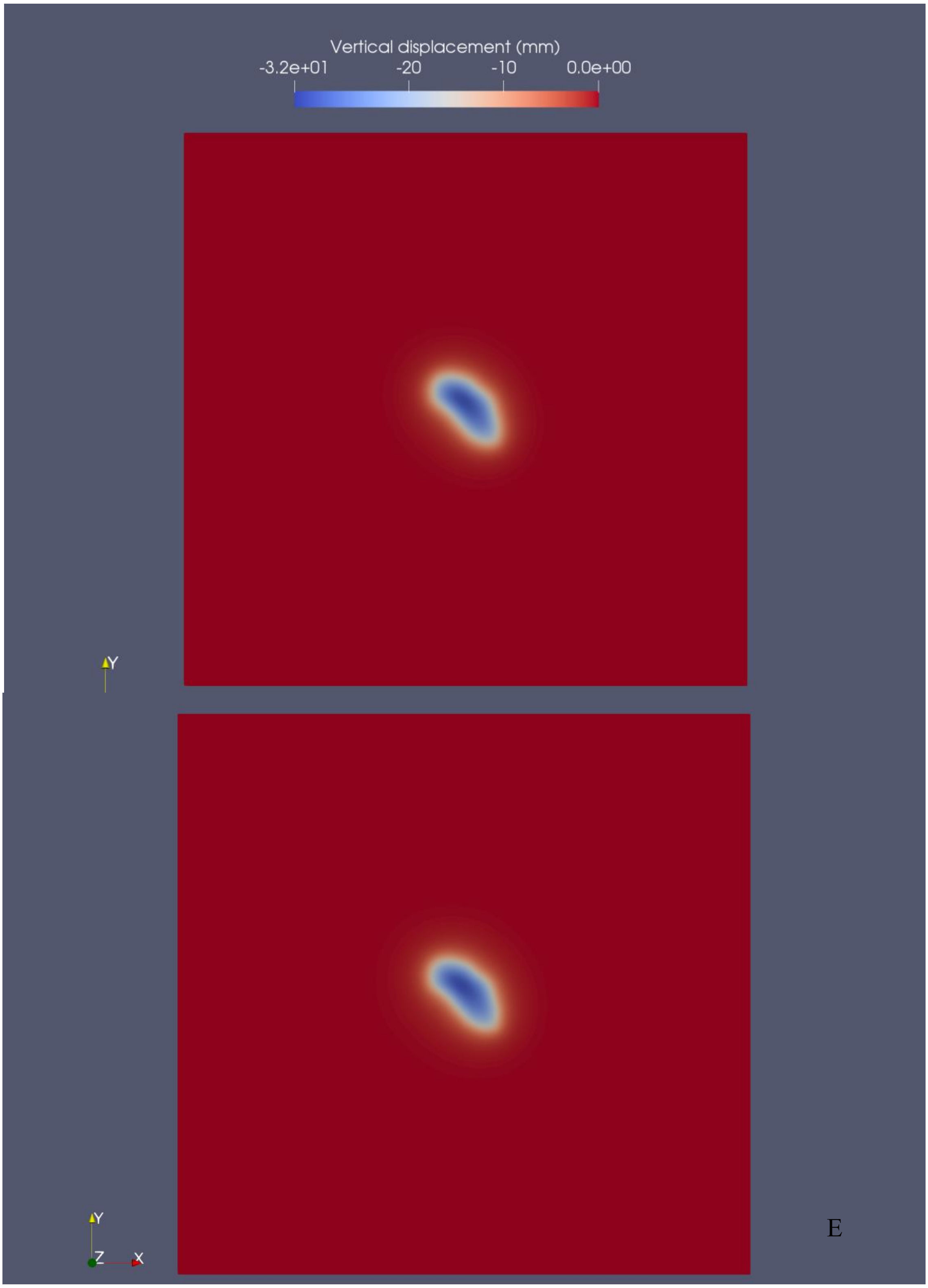

Fig. 4.31: Top View displaying the approximated subsidence over the whole geomechanical volume: A) FEM solution and E) VEM solution over the Hybrid mesh (ParaView Visualization).

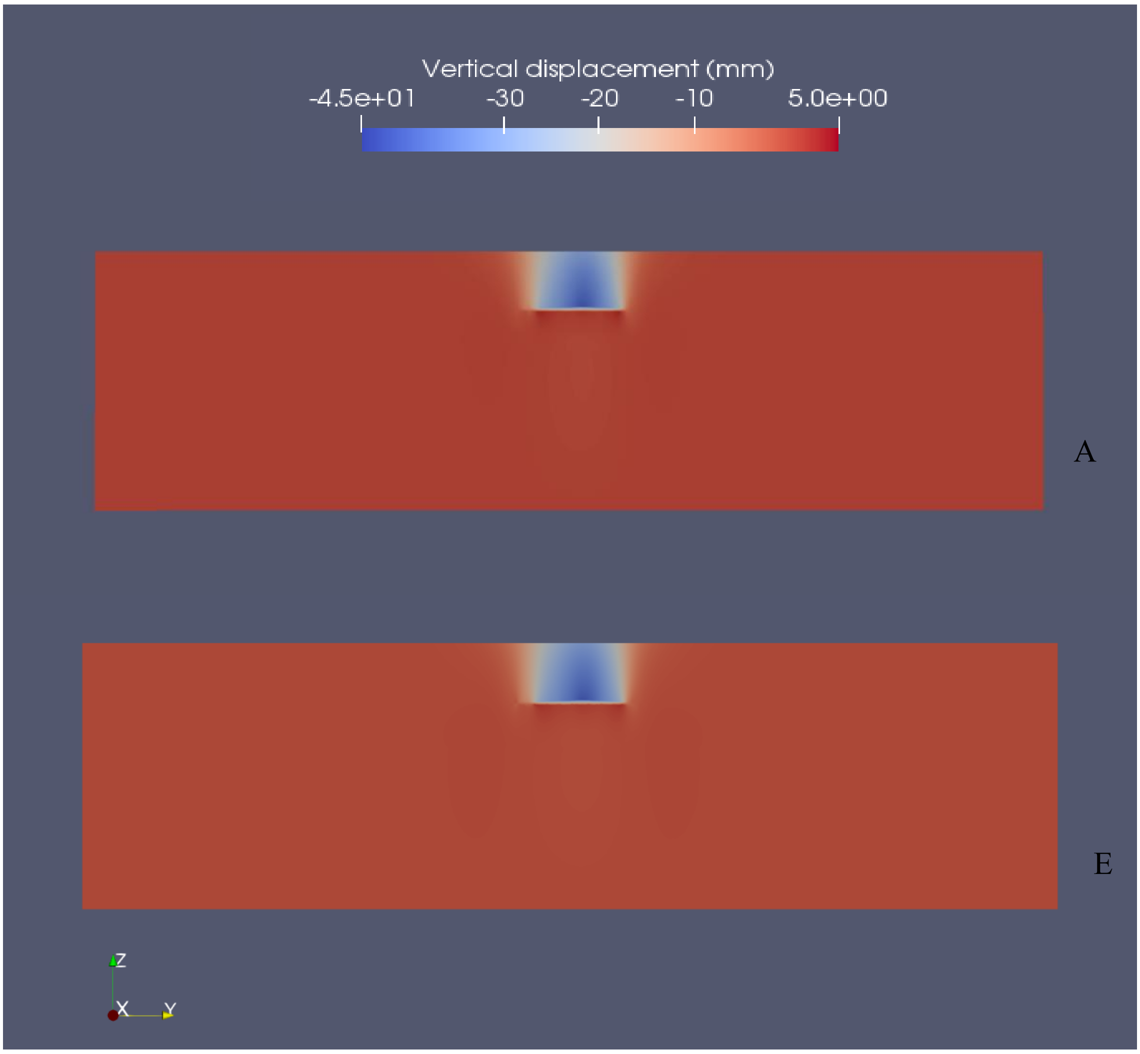

Fig. 4.32: Vertical section approximated displacements (along the z-axis) over the whole geomechanical volume: A) FEM solution and E) VEM solution over the Hybrid mesh (ParaView Visualization).

Tab. 4.12: Summary of Calculated displacements of VEM solution over the hybrid mesh.

	FEM solution	**VEM solution over the hybrid mesh**
Maximum displacement at the surface (subsidence) in mm	-30.8897	-31.0086
Maximum displacement over the whole volume in mm	-42.7726	-42.4803

For this volume discretization scenario, the VEM computes accurate results with a discrepancy range within the order of 10^{-1} millimeters over the whole volume and the computed subsidence as well. In this case, the hybrid mesh is refined 12 times more than the mesh with split faced-polyhedra, confirming the previous hypothesis: for a load factor concentrated at the reservoir level, the polyhedral discretization is too coarse for VEM to compute accurately the stress variations and consequently the displacements.

Summary:

Tab. 4.13: Summary of Calculated displacements by VEM.

	FEM solution	**VEM solution with respect th discretization scenario**			
		Unstructured mesh	**Structured grid**	**Structured grid with general polyhdera**	**Hybrid grid**
Maximum displacement at the surface (subsidence) in mm	-30.8897	-33.1450	-4.4969	-10.7809	-31.0086
Maximum displacement over the whole volume in mm	-42.7726	-45.4396	-5.9624	-15.3301	-42.4803

Considering the various discretization scenarios, we confined our comparison of solution discrepancy to the assessment of the degree of magnitude of displacements between VEM and FEM solutions and how the phenomena is properly simulated. Because, when working with these different grids: the coordinates of nodes and centroids and their respective number differ from one scenario to another; rendering the nodal analysis of solutions challenging. For each grid a different comparison workflow must be adopted against FEM solution solved under Petrel's regular structured grid. This new step introduces additional numerical/geometrical variables specific to each scenario that have be considered when analyzing the discrepancies. It can hinder the integrity of the overall study for time being. Prompting us to rely only on the assessment of the degree magnitudes.

5. Conclusion

The effects of volume discretization on the Virtual Element Method (VEM) in simulating the subsidence phenomena induced by gas production bearing formation were tested and analyzed. A synthetic model was constructed, representative of an offshore gas reservoir within the Northern part of the Adriatic Sea. The anticlinal topology of the formation has provided us with meshing scenarios to investigate the sensitivity of the implemented first order Virtual Element scheme. The computed values were compared against an 8 node isoparametric hexaedron FEM Geomechanics® solution taken as reference.

We described briefly the workflow adopted to pass the 3D Geomechanical model from the FEM commercial software to the VEM simulator, highlighting the processing steps followed during data export.

Before starting our analysis, we employed a simplified synthetic model in order to assess the solution discrepancy factors that are solver dependent: data extrapolation methods and boundary conditions. Through the use of a regular hexahedral structured grid, we showed that the VEM gives accurate results when simulating a displacements field with negligible discrepancy less than 1% from the FEM solution.

Once the minimum expected solution discrepancy was established, we applied the VEM method over the realistic model. At first, we ran the VEM method on a tetrahedral unstructured grid. The mesh proved to be adequate in terms of degree of refinement and implicit satisfaction of planarity. Thus, the subsidence was properly represented.

Next we showed that, when used directly on the original Petrel's structured grid, the VEM fails to provide comparable results. In particular, because of the curvature of the anticline, the resulting hexahedral cells have non-planar faces, posing a difficulty for the VEM to properly transfer the displacements.

Once we converted cells into polyhedra by splitting not-planar faces in triangles, we observed an improvement in the computed subsidence (doubled values), but yet it was still largely underestimated. So, we sought out to improve the precision of the computation at the reservoir level by increasing the number of cells. At this purpose the previously defined polyhedral cells were split into tetrahedra.

The resulting grid became an hybridization of the original corner point grid and an unstructured mesh identified by tetrahedral cells at the reservoir level. Results comparison was now satisfying with a discrepancy with FEM reference solution even lower than the ones obtained from unstructured meshing.

Conclusion remarks

- The tested VEM scheme can provide an accurate prediction of the subsidence phenomena depending on the mesh discretization (tetrahedral unstructured grid vs corner point gridding)
- We confirmed that influence of not-planar cell faces has a not negligible effect on the displacement calculated through the actual implementation of the VEM
- The implemented VEM scheme, based on first order approximation, requires a grid refinement such as the introduction of tetrahedral element in order to reproduce a solution which has an accuracy comparable with the tested first order FEM based on 8 node isoparametric brick element.

Since the present analysis pointed out the intrinsic limitations in directly applying the first order VEM to corner point grids, in future work a grid optimization algorithm, in terms of faces planarization and refinement, will be investigated in order to be able to perform reliable simulations on such kind of meshes which represents a well-established output of geological modelling workflow.

References:

[1] Gould, Phillip L. Introduction to Linear Elasticity. 3rd ed. New York: Springer, 2013. Print.

[2] Fjar, Erling, R.M. Holt, A.M. Raaen, R. Risnes, and P. Horsrud. Petroleum Related Rock Mechanics. 2nd ed. Vol. 53. Elsevier Science, 2008. Developments in Petroleum Science. Print.

[3] Mark D.Zoback. Reservoir Geomechanics, (2007). Print

[4] Andi Merxhani, An introduction to linear poroelasticity, 2016. 1607.04274. https://arxiv.org/abs/1607.04274v1

[5] C. Deangeli, Reservoir Geomechanics course lecture, 2017. Politecnico Di Torino.

[6] Oilfield Review Autumn 2006, COmpaction and subsidence, https://www.slb.com/resources/oilfield_review/en/2006/or2006_aut.aspx

[7] Settari, A. (2002, August 1). Reservoir Compaction. Society of Petroleum Engineers. doi:10.2118/76805-JPT

[8] Geertsma, J. (1973, June 1). Land Subsidence Above Compacting Oil and Gas Reservoirs. Society of Petroleum Engineers. doi:10.2118/3730-PA

[9] Hettema, M. H. H., Schutjens, P. M. T. M., Verboom, B. J. M., & Gussinklo, H. J. (2000, August 1). Production-Induced Compaction of a Sandstone Reservoir: The Strong Influence of Stress Path. Society of Petroleum Engineers. doi:10.2118/65410-PA

[10] Reddish, D. J., Yao, X. L., & Waller, M. D. (1994, January 1). Computerised prediction of subsidence over oil and gas fields. Society of Petroleum Engineers. doi:10.2118/28105-MS

[11] Anna Szostak-Chrzanowski, Adam Chrzanowski, Eulalio Ortiz, (2006), MODELING OF GROUND SUBSIDENCE IN OIL FIELDS, Canadian Centre for Geodetic Engineering (CCGE), University of New Brunswick.

[12] P.A.Fokker (2001, WIT Press). Semi-analytical subsidence prediction. Netherlands Institute of Applied geoscience TNO. ISSN 1743-355X.

[13] Romeu, R. K., Paraizo, P. L. B., Moraes, M. A. S., Lima, C. B., Lopes, M. R. F., Silva, A. T., … Damiani, M. C. (2005, January 1). Reservoir Representation for Flow Simulation. Society of Petroleum Engineers. doi:10.2118/94735-MS

[14] Samier, P., & De Gennaro, S. (2007, January 1). Practical Iterative Coupling of Geomechanics With Reservoir Simulation. Society of Petroleum Engineers. doi:10.2118/106188-MS

[15] Settari, A., & Walters, D. A. (2001, September 1). Advances in Coupled Geomechanical and Reservoir Modeling With Applications to Reservoir Compaction. Society of Petroleum Engineers. doi:10.2118/74142-PA

[16] Samier, P., & De Gennaro, S. (2007, January 1). Practical Iterative Coupling of Geomechanics With Reservoir Simulation. Society of Petroleum Engineers. doi:10.2118/106188-MS

[17] Yale, D. P., Lyons, S. L., & Qin, G. (2000, January 1). Coupled Geomechanics-Fluid Flow Modeling in Petroleum Reservoirs: Coupled Versus Uncoupled Response. American Rock Mechanics Association.

[18] Thomas, L. K., Chin, L. Y., Pierson, R. G., & Sylte, J. E. (2002, January 1). Coupled Geomechanics and Reservoir Simulation. Society of Petroleum Engineers. doi:10.2118/77723-MS

[19] Gutierrez, M. (1994, January 1). Fully Coupled Analysis of Reservoir Compaction and Subsidence. Society of Petroleum Engineers. doi:10.2118/28900-MS

[20] A. Settari , D. A. Walters , D. H. Stright Jr. & K. Aziz (2008) Numerical Techniques Used for Predicting Subsidence Due to Gas Extraction in the North Adriatic Sea, Petroleum Science and Technology, 26:10-11, 1205-1223, DOI: 10.1080/10916460701833889

[21] A Coupled Fluid Flow - Geomechanical Approach for Subsidence Numerical Simulation / Giani, Grazia; Orsatti, Serena; Peter, Costanzo; Rocca, Vera. - In: ENERGIES. - ISSN 1996 1073. - ELETTRONICO. - 11(2018), pp. 1-17.

[22] Jalali, Mohammadreza, Dusseault, Maurice, Coupling Geomechanics and Transport in Naturally Fractured Reservoirs, International Journal of Mining and Geo-Engineering, 2012/12/01

[23] J. N. Reddy, "An Introduction to the Finite Element Method," 2nd Edition, McGraw-Hill, New York, 1993.

[24] W. Fred Ramirez, Chapter 8 - SOLUTION OF PARTIAL DIFFERENTIAL EQUATIONS, Computational Methods in Process Simulation (Second Edition), Butterworth-Heinemann,1997, Web.

[25] G. P. Nikishkov, INTRODUCTION TO THE FINITE ELEMENT METHOD, University of Aizu, Aizu-Wakamatsu 965-8580, Japan.
[26] Rashid, M. M. and Selimotic, M. (2006), A three-dimensional finite element method with arbitrary polyhedral elements. Int. J. Numer. Meth. Engng., 67: 226-252. doi:10.1002/nme.1625
[27] Arun L.GainaGlaucio H.PaulinoabLeonardo S.DuartecIvan F.M.Menezesc , Topology optimization using polytopes a Department of Civil & Environmental Engineering, University of Illinois at Urbana-Champaign, USA b School of Civil and Environmental Engineering, Georgia Institute of Technology, USA c Tecgraf, Pontifical Catholic University of Rio de Janeiro (PUC-Rio), Brazil, Computer Methods in Applied Mechanics and Engineering Volume 293, 15 August 2015, Pages 411-430
[28] Beirao da Veiga, L & Brezzi, Franco & Cangiani, Andrea & Manzini, Gianmarco & D. Marini, L & Russo, Alessandro. (2012). Basic principles of Virtual Element Methods. Mathematical Models and Methods in Applied Sciences. 23. 10.1142/S0218202512500492.
[29] Antonietti, P.F.; Beirao da Veiga, L.; Mora, D.; Verani, M. A stream virtual element formulation of the Stokes problem on polygonal meshes MOX, Dipartimento di Matematica “F. Brioschi” Politecnico di Milano, Via Bonardi 9 - 20133 Milano (Italy)
[30] Beirao da Veiga, L & Brezzi, Franco & Marini, L.D. & Russo, Alessandro. (2014). The Hitchhiker's Guide to the Virtual Element Method. Mathematical Models and Methods in Applied Sciences. 24.10.1142/S021820251440003X.
[31] Virtual Element Method Course project of Advanced Numerical Analysis of Partial Differential Equations (Prof. S. Perotto), and Advanced Programming for Scientific Computing (Prof. L. Formaggia)
[32] Konstantin Lipnikov, Gianmarco Manzini, Mikhail Shashkov. Mimetic finite difference method. Journal of Computational Physics, Volume 257, Part B, 2014. ISSN 0021-9991, https://doi.org/10.1016/j.jcp.2013.07.031.
[33] Benetatos C., Viberti D. (2010). Fully Integrated Hydrocarbon Reservoir Studies: Myth or Reality? In: AMERICAN JOURNAL OF APPLIED SCIENCES, vol. 7 n. 11, pp. 1477-1486. ISSN 1546-9239.

[34] Andersen, O., Nilsen, H.M. & Raynaud, X. Virtual element method for geomechanical simulations of reservoir models Comput Geosci (2017) 21: 877. https://doi.org/10.1007/s10596-017-9636-1
[35] Gringarten, E., Lecuyer, J. D., Villarubias, E., Cosson, C., & Li, W.-C. (2017, October 9). Optimized Grids for Accurately Representing Geology in Geomechanical Simulations. Society of Petroleum Engineers. doi:10.2118/187299-MS
[36] Andersen, O., Nilsen, H. M., & Raynaud, X. (2017, February 20). Coupled Geomechanics and Flow Simulation on Corner-Point and Polyhedral Grids. Society of Petroleum Engineers. doi:10.2118/182690-MS
[37] Visage User's Guide, Shlumberger
[38] VTK User's Guide, Free Available Section ''File Format for VTK version 4.2''
[39] Overview of the Italy's Petroleum Systems and Related Oil and Gas Occurences F. Bertello* (ENI - Exploration and Production Division), R. Fantoni (ENI - Exploration and Production Division) & R. Franciosi (ENI - Exploration and Production Division), 70th EAGE Conference & ExhibitionAt: FirenzeVolume: Extended Abstract & Exhibitor's Catalogue, June 2008, DOI: 10.3997/2214-4609.20147556
[40] Cazzini, F., Zotto, O. D., Fantoni, R. , Ghielmi, M. , Ronchi, P. and Scotti, P. (2015), OIL AND GAS IN THE ADRIATIC FORELAND, ITALY. Journal of Petroleum Geology, 38: 255-279. doi:10.1111/jpg.12610
[41] Bresciani, I., and Perotti, C. R. (2014), An active deformation structure in the Po Plain (N Italy): The Romanengo anticline, Tectonics, 33, 2059– 2076, doi:10.1002/2013TC003422.
[42] Malvić, T., Đureković, M., Šikonja, Ž., Čogelja, Z., Ilijaš, T., & Kruljac, I. (2011). Exploration and Production Activities in northern Adriatic Sea (Croatia), successful joint venture INA (Croatia) and ENI (Italy).